Transition from quantum to classical dynamics in weak measurements and reconstruction of quantum correlation

Vadim V. Vorobyov [1,*] Jonas Meinel,[1,2] Hitoshi Sumiya,[3] Shinobu Onoda,[4] Junichi Isoya,[5] Oleg Gulinsky,[6,†] and Jörg Wrachtrup[1,2,‡]

[1]*3rd Institute of Physics, IQST and Centre for Applied Quantum Technologies, University of Stuttgart, 70569 Stuttgart, Germany*
[2]*Max-Planck Institute for Solid State Research, 70569 Stuttgart, Germany*
[3]*Advanced Materials Laboratory, Sumitomo Electric Industries Ltd., Itami 664-0016, Japan*
[4]*Takasaki Advanced Radiation Research Institute, National Institutes for Quantum and Radiological Science and Technology, Takasaki 370-1292, Japan*
[5]*Faculty of Pure and Applied Sciences, University of Tsukuba, Tsukuba 305-8573, Japan*
[6]*F. Riesz Center for the Study of the Foundations of Classical and Quantum Probability, Netanya 4226728, Israel*

The ability to track and control the dynamics of a quantum system is the key to quantum technology. Despite its central role, the quantitative reconstruction of the dynamics of a single quantum system from the macroscopic data of the associated observable remains a problem. We consider this problem in the context of weak measurements of a single nuclear carbon spin in a diamond with an electron spin as a meter at room temperature, which is a well-controlled and understandable bipartite quantum system. In this work, based on a detailed theoretical analysis of the model of the experiment, we study the relationship between the statistical properties of the macroscopic readout signal of the spin of a single electron and the quantum dynamics of the spin of a single nucleus, which is characterized by a parameter associated with the strength of the measurement. We determine the parameter of measurement strength in separate experiments and use it to reconstruct the quantum correlation. We control the validity of our approach applying the Leggett-Garg test.

I. INTRODUCTION

The advantage of quantum information systems is based on the ability to store and process information encoded in a set of qubits. An obstacle to the implementation of complex quantum algorithms is the decoherence effect that occurs in the process of interaction and transformation of information. To transfer information from one subsystem of a complex system to another, both subsystems must be entangled, which inevitably leads to irreversible state changes and loss of information. The ability to track and control the dynamics of a quantum system is the key to quantum technology.

To the best of our knowledge, it is impossible to completely and unambiguously restore the state of quantum systems based on the macroscopic measurements of observables associated with the system. In principle, the state of a quantum system can be characterized using the Wigner distribution function. However, the reconstruction procedure for this function is extremely sensitive to measurement errors, is inefficient, and requires a large number of experiments [1,2]. In this work, we pose a more modest problem of restoring the correlation function of the dynamics of an observable associated with a quantum object. We control the accuracy of

our reconstruction by checking the nonclassical properties of the resulting correlation function using the Leggett-Garg test.

In contrast to the classical filtering and control problem, the main difficulty in the quantum case is that the probabilistic properties of the classical (macroscopic) process at the output of the system and the quantum process that generates it differ significantly (see, e.g., [3,4]). In this regard, it is interesting to trace theoretically the transformation of a quantum process into a macroscopic output process and test this analysis with experimental results on a simple model. On this path, we are guided by the idea that measurements are not an instantaneous jumplike act (collapse of the wave function), but a process in which one quantum state is replaced by another, pure or mixed, under the control of some interaction Hamiltonian, while the final stage of this process is just a nonunitary nature (see Sec. III B).

The classical probability measure $\mathbb{P}$ is defined on the probability space $(\Omega, \mathscr{F})$ or, equivalently, on a Boolean algebra $\mathscr{A}$ (distributive lattice) and satisfies the strong additivity property

$$\mathbb{P}(A) + \mathbb{P}(B) = \mathbb{P}(A \wedge B) + \mathbb{P}(A \vee B), \quad A, B \in \mathscr{A}. \quad (1.1)$$

On the other hand, the quantum probability is defined on an orthomodular (nondistributive) lattice generated by projections of a Hilbert space, where a finite function (dimension function) with a property similar to (1.1) exists only in special cases (see [5,6]). Moreover, there is no dispersion free state (corresponding to the δ measures in classical case) on a complex Hilbert space of dimension greater than two (Gleason's

theorem [7]; see also [8]). In other words, randomness is an inevitable property of quantum states.

Strong additivity is a distinctive property that fundamentally separates classical probability from quantum probability, which manifests itself in a variant of the proof of Wigner's and d'Espagnat's formulation [9,10] for Bell's theorem, given for clarity in Appendix A.

Bell [11,12], using Bohm's version [13] (ch. 22) of the Einstein-Podolsky-Rosen (EPR) arguments [3], introduced test inequalities relating correlations between measurements in separate parts of the classical composite system. While Bell's inequalities examine correlations of bounded random variables over space, the more recent Leggett-Garg inequality [14] examines correlations over time. The simplest Bell- and Leggett-Garg-type inequalities can be represented in the same form,

$$C_{21} + C_{32} - C_{31} \leqslant 1,$$

where C_{ij} are the two-point correlation functions with different pairs of space or time arguments. This inequality limits the strength of spatial or temporal correlations that can arise in a classical framework and is expected to be violated by quantum mechanical unitary dynamics such as Rabi oscillations or Larmor precession.

From a mathematical point of view, Bell-type inequalities arose in classical probability more than 100 years before Bell's discovery. The first appearance of such a result is associated (see [15,16]) with the name of the creator of Boolean algebra [17]. The final solution to this problem is formulated as Kolmogorov's consistency theorem (see, e.g., [18]). The key mathematical condition of Bell-type theorems is that all (bounded) random variables given in space or in time are defined on the same probability space, which is especially significant in the case of spatially separated subsystems in the Bell test. In terms of applicability, a critical limitation of Bell-type theorems is that inequalities are derived under the assumption of noninvasive measurements.

We consider the tracking problem in the framework of measurements of a single nuclear spin in a diamond with an electron spin as a meter at room temperature [19–21]. This is a well-controlled and understandable bipartite quantum system. A feature of a substitutional nitrogen nuclear spin is that it lies on the nitrogen-vacancy (NV) axis, and therefore its hyperfine tensor is rotationally symmetric and collinear with the NV axis.

The possibility of quantum nondemolition (QND) measurement of single nitrogen nuclear spins (^{14}N, ^{15}N) to probe different charge states of the NV center was demonstrated in [22]. In this case, the system observable is the nuclear spin I_z, which undergoes the Rabi oscillations, while the probe observable is the electron spin S_z. This is a realizable QND, which is close to the conditions of projective measurement [23].

Tracking the precession of a single nuclear ^{13}C spin using periodic weak measurements was demonstrated in [24,25]. The nuclear spin of carbon in diamond weakly interacts with the electron spin of a nearby nitrogen vacancy center, which acts as an optically readable measurement qubit. The nuclear spin undergoes a free precession around the z axis with an angular velocity given by the Larmor frequency ω. The pre-

cession is monitored by probing the nuclear spin component I_x by means of a conditional rotation via the effective interaction Hamiltonian $H \approx A_{\parallel} S_z I_x$, which couples I_x with the S_z component of electronic spin.

The experimental setup of our work basically coincides with the scheme of [24]. However, the problem of restoring the correlation function of a quantum signal from the data of successive (weak) measurements and, in particular, the subsequent application of the Leggett-Garg test required a significant development of the experiment and an increase in the measurement accuracy.

To the best of our knowledge (see [15,26]), most of the experiments on the application of the Leggett-Garg test used explicit or implicit preprocessing of macroscopic experimental data (application of an empirical "measurement factor," filtering, postselection). For example, Palacios-Laloy *et al.* [27] wrote (we adhere to the original notations): "under macrorealistic assumptions, the only effect of the bandwidth of the resonator would be to reduce the measured signal by its Lorentzian response function $C(\omega) = 1/[1 + (2\omega/k)^2]$; we thus have to correct for this effect by dividing the measured spectral density $\tilde{S}_z(\omega)$ by $C(\omega)$. We then compute $K(\tau)$ by inverse Fourier transform of $S_z(\omega) = \tilde{S}_z(\omega)/C(\omega)$." Palacios-Laloy *et al.* found that their qubit violated Leggett-Garg tests, albeit with a single data point, and conclude that their system does not admit a realistic, noninvasively measurable description.

In Waldherr *et al.* [28] the data preprocessing procedure is explicitly described. They reconstruct the conditional Rabi oscillation for a substitutional nitrogen nuclear spin using (almost) projective QND measurements [22]. The application of a narrow-band, nuclear spin state-selective microwave π pulse flips the electron spin into the $|+1\rangle_e$ state or $|0\rangle_e$ and $|-1\rangle_e$ states conditional on the state of the nuclear spin. However, only if the measurement outcome is $|+1\rangle_n$ is the Rabi oscillation generated. Since the fluorescence intensity differs significantly for the electron spin states $|+1\rangle_e$ (low) and $|0\rangle_e$ and $|-1\rangle_e$ (high), these target states can be distinguished in the histogram of many subsequent measurements using a maximum likelihood statistical procedure. Low fluorescence level indicates that the π pulse was successful, i.e., that the nuclear spin state is $|+1\rangle_n$. Only in this successful case is a resonant radio-frequency pulse of certain length applied and a subsequent measurement is used for data analysis.

In our experiment (see Sec. II), the successive weak measurements generate a classical stochastic signal whose characteristics can be calculated using a positive operator-valued measure (POVM) measurement scheme. We theoretically show that the correlation of the classical output signal can be converted to the correlation of nuclear spin dynamics using a mapping dependent on the factor α characterizing the strength of the measurements. A similar idea of applying inverse imaging to macroscopic data has been used in the field of quantum tomography (see, e.g., Smithey *et al.* [1]).

We apply the theoretical mapping to the output classical process (or, equivalently, to the empirical correlation function) in order to recover the correlation function of the quantum object. Only then do we apply the Leggett-Garg inequality to verify that the reconstructed process violates the classical properties of correlations. Thus, although the Leggett-Garg
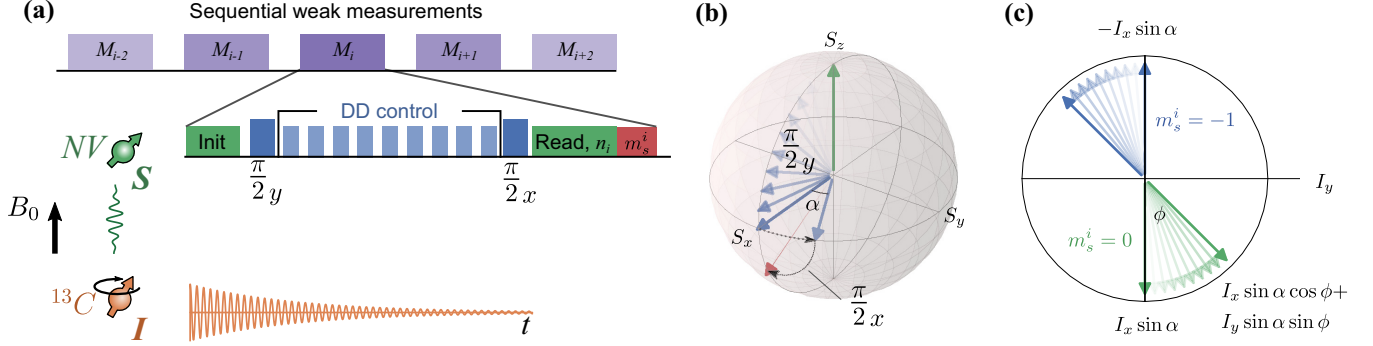
FIG. 1. Scheme of the experiment. (a) The sequential weak measurements M_i are composed of a sensor initialization part, dynamical decoupling (KDD-XYn), and readout of the sensor state using conventional optical readout of an NV center electron spin. The KDD-XYn filter function is tuned via pulse spacing τ to the Larmor precession of the weakly coupled ($A_{zz} \approx 100$ Hz) ^{13}C nuclear spin, which results in an effective interaction between nuclear and electron spin. The electron spin state is read out after each interaction, which leads to extraction of information about the nuclear spin and its back-action. (b) Schematic evolution trajectory of an electron spin state in the case the nuclear spin is in the $I_e + I_x$ state (c) Schematic evolution of the nuclear spin during sequential measurements. Initially, the nuclear spin is in the thermally mixed state $\rho_0 = I_e$, which is then partially polarized by measurements along the x axis with magnitude $\sin \alpha$. The free precession between the measurements leads to a rotation around the z axis, which is perpendicular to the figure plane. Subsequent measurements affect the measurement by disturbing both the x and y component of the Bloch vector, conditioned on the measurement outcome (see text).

test was not developed for invasive (albeit weak) measurements, our approach allowed us to apply it to verify the compliance of the model and the method of analysis with the experimental conditions.

Moreover, our approach makes it possible to introduce an analog of the classical relative entropy of Kullback and Leibler as a measure of the discrepancy of information that occurs during the measurement process. This definition differs from the relative entropy commonly used in the noncommutative case.

The paper is organized as follows. A detailed description of the main experiment and the results are given in Sec. II, while the theoretical analysis is carried out in Sec. III.

The main tools of our analysis are the POVM measurements theory and the Baker-Campbell-Hausdorff (BCH) formula. We introduce a modification of closed form (3.12) of the BCH formula (a simple proof is given in Appendix B) and show that it can be used in our model. In view of the numerous references in our main text to various aspects of the POVM theory, we found it useful to summarize for convenience the main facts of this theory in Appendix C.

II. EXPERIMENT AND RESULTS

A. Experimental setup

We use a single ^{13}C nuclear spin in diamond as quantum system, probed by an NV center electron spin [see Fig. 1(a)]. The electron spin interacts weakly with the single ^{13}C nuclear spin through their hyperfine interaction. Each NV electron spin can selectively address nuclear spins in the near vicinity under control of the dynamical decoupling (DD) sequence and is then read out using projective optical measurements (see Appendix K for details).

B. Model and main assumptions

Recall that the secular hyperfine vector $\mathbf{A}_z$ of the hyperfine tensor $\mathbf{A}(\mathbf{r})$, $\mathbf{r} = (r, \theta, \phi)$ with a properly chosen x axis is

given by

$$\mathbf{A}_z = (A_{xz}, 0, A_{zz}) = (A_\perp, 0, A_\parallel). \tag{2.1}$$

Since the electronic spin precesses at a much higher frequency than the nuclear spin, the nuclear feels only the static component of the electronic field. Therefore, the dynamics of the unified system with single spin ^{13}C can be described by the Hamiltonian in the secular approximation:

$$H = \omega I_z + 2\pi A_\parallel S_z \otimes I_z + 2\pi A_\perp S_z \otimes I_x, \tag{2.2}$$

where $\omega_L = \gamma_C B_z$, γ_C is the ^{13}C gyromagnetic ratio, B_z is the external magnetic field along the NV axis, S_z, I_x, I_z are the electron and nuclear spin-1/2 operators, and $A_\parallel = A_{zz}$ and $A_\perp = \sqrt{A_{xz}^2 + A_{yz}^2}$ are the parallel and transverse hyperfine coupling parameters. After the interaction controlled by the Hamiltonian and the DD sequence, the amplitude of the nuclear component I_x is mapped to optically detectable component S_z of the NV center.

In our experiment, the interaction between the electron and nuclear spins is controlled by a Knill-dynamical decoupling (KDD-XYn) sequence of periodically spaced π pulses, which contains n units of 20 pulses with a pulse interval τ. The measurement strength of weak measurements can be varied. If τ is adjusted to the effective nuclear Larmor period ω_L, that is (see [20]),

$$\tau = \frac{(2k+1)\pi}{2\omega_L + 2\pi A_{zz}}, \quad \text{if } 2\pi A_{zx} \ll \gamma_n B \tag{2.3}$$

or

$$\tau = \pi/\omega_L \quad \text{if } 2\pi A_{zz} \ll \omega_L, \tag{2.4}$$

we can assume that the system evolves under the effective Hamiltonian [24,29,30]

$$H_{\text{eff}} = 2\alpha S_z \otimes I_x, \tag{2.5}$$

where the Larmor frequency is determined by the static magnetic field (in our experiment $B \approx 0.25$ T). The effect of the KDD-XYn sequence is specified by a measurement strength

parameter $\alpha = \pi N_p A_\perp \tau$, which depends on the transverse hyperfine component $A_\perp$ and the number of pulses $N_p = 20n$.

Nuclear-spin precession at the Larmor frequency around an external magnetic field **B** is perturbed by the presence of the electron spin. As a result, depending on the NV charge and spin states NV$^-$, $m_S = \{-1, 0, +1\}$ or NV^0, $m_S = \{-1/2, +1/2\}$, the precession frequency and axis are modified. The interaction Hamiltonian gives rise to electron-spin-dependent nuclear precession frequencies ω_0 (electron spin in $|0\rangle$) and $\omega_{\pm 1} = \sqrt{(\omega_0 \pm a_\parallel)^2 + a_\perp^2}$ (electron in $|m_S = \pm 1\rangle$, $a_\parallel = 2\pi A_\parallel$, $a_\perp = 2\pi A_\perp$). The interaction controlled by the effective Hamiltonian H_{eff} carries the main information about the nuclear spin through the transverse hyperfine component $A_\perp$, but introduces a dephasing associated with the back-action on the nuclear spin. At the same time, the secular *longitudinal part* of the hyperfine interaction $A_\parallel S_z \otimes I_z$ turns out to be a source of significant information distortion.

C. Influence of the longitudinal part: Diamond sample

One of the possible mechanisms for involving the longitudinal component $A_\parallel$ into the dynamics in our experiment is the process of optical readout [25]. During optical readout of the NV center with *nonresonant* laser pulse, due to the shift $\triangle \omega = |\omega_0 - \omega_{\pm 1}|$ of nuclear precession, the NV center cycles through its electronic states before reaching the $m_S = 0$ spin-polarized steady state. The way to overcome the influence of the surrounding nuclear spins ^{13}C on the sample spin is to reduce the concentration of nuclear spins ^{13}C. To this end, our experiment is carried out at NV centers in *isotopically purified diamond* (see Appendix K).

Uncontrolled dynamics of electron spin states during and after the readout leads to random z rotations of the nuclear spin under the action of the secular *longitudinal part* of the hyperfine interaction $A_\parallel S_z \otimes I_z$. Therefore, due to a random phase accumulation, stochastic flips of the sensor spin lead to the decoherence of target spin with the intrinsic transverse relaxation time T_2^* or the intrinsic nuclear dephasing rate $\Gamma_{intr} = (T_2^*)^{-1}$ It is also believed that the longitudinal hyperfine interaction during laser readout causes an additional dephasing with rate [25]

$$\Gamma_{opt} \approx \frac{A_\parallel^2 t_l^2}{2 t_s}, \qquad (2.6)$$

where $t_l = t_{\text{readout}}$ is a period at which $m_s \neq 0$ and t_s is a sample time.

The influence of the *longitudinal part* of the hyperfine interaction $A_\parallel S_z \otimes I_z$ associated with optical readout accumulates with an increase in the number of measurements. As a result, a short period of weakly perturbed behavior does not make it possible to reveal the purely quantum properties of the nuclear spin. Therefore, for the purposes of our experiment, it is desirable to choose a pair of NV-nuclear spins for which the value of $A_\parallel$ is negligibly small. The properties of the various electron-nuclear pairs and the process of choosing a suitable pair are described in more detail in Appendix J. In our diamond sample, we managed to find such a pair corresponding to "the magic angle cone," which made it possible to obtain a clear picture of the interaction.

D. Detection protocol

We now turn to the description of the results of the experiment with this particular magic pair, designated as NV2. In our experiment, we investigated both prepolarized and nonpolarized initial conditions for the nuclear spin. While electron spin polarization is a relatively easy task, nuclear spin polarization is a rather delicate procedure. In the main text, we analyze and present the main results for the partially polarized case, when incomplete polarization occurs during the first measurements (see Sec. III D). The results for the case of a prepolarized target spin are presented in Appendix G for additional information.

When initially the nuclear spin is not polarized, it is represented by a completely mixed state

$$\rho_I = \tfrac{1}{2}|0\rangle\langle 0| + \tfrac{1}{2}|1\rangle\langle 1| = \tfrac{1}{2}I^\alpha + \tfrac{1}{2}I^\beta = \tfrac{1}{2}\mathbb{1} = I_e, \quad (2.7)$$

where $I^\alpha = I_e + I_z$, $I^\beta = I_e - I_z$ and $I_e = \tfrac{1}{2}\mathbb{1}$, $S_k = I_k = 1/2\,\sigma_k$, and σ_k are Pauli matrices. In Sec. III D, we show that the initial state (2.7) during the first measurements is transformed into a partially polarized state $I_e + \sin\alpha I_x$, the degree of polarization of which depends on the parameter α.

The measurement protocol is as follows. The electron spin is optically pumped [see Figs. 1(a) and 1(b)] into the state $|0\rangle = |m_S = 0\rangle$ or equivalently to $S_e + S_z$, and then rotated by a $(\pi/2)_y$ pulse around the y axis to state $S_e + S_x$. Then the interaction controlled by the KDD-XYn sequence is applied, which ends with a $(\pi/2)_x$ pulse along the x axis. Between two successive measurements the target spin undergoes free precession around the z axis with the Larmor frequency ω_L [see Fig. 1(c)], during which the accumulation of information about the target object takes place. The final optical readout of the S_z component of the NV sensor repolarizes the sensor back to the initial state $S_e + S_z$ while maintaining the nuclear spin state in the x-y plane, which reduces the amplitude of the I_y component by a factor of $\cos\alpha$. Nuclear precession leads to a mixing of the I_x and I_y amplitudes. Thus, in the process of measurement, the components I_x and I_y are subject to a back-action, which leads to an exponential decay of the spin amplitude, depending on the strength parameter α.

E. Data analysis

The experiment is designed in such a way that the interaction Hamiltonian (the effective Hamiltonian proportional to $S_z \otimes I_x$) and density matrices are expressed in terms of operators S_i and I_j of the basis (3.3) so the dynamics of the object can be calculated using a modification of the Baker-Campbell-Hausdorff (BCH) formula (3.12).

An analysis of the transformation of the state of the composite system and, in particular, the dynamics of the state of the target nuclear spin during the interaction is given in Sec. III B. We single out the moment when, as a result of the interaction of the NV center as a meter with the spin ^{13}C, the amplitude of the observable I_x is mapped into the observable S_y and next to S_z after a $\pi/2$ pulse along S_x axis with the inevitable uncertainty introduced by the factor $\sin\alpha$, which characterizes the strength of the interaction. Together with the projective measurement, this process converts the quantum
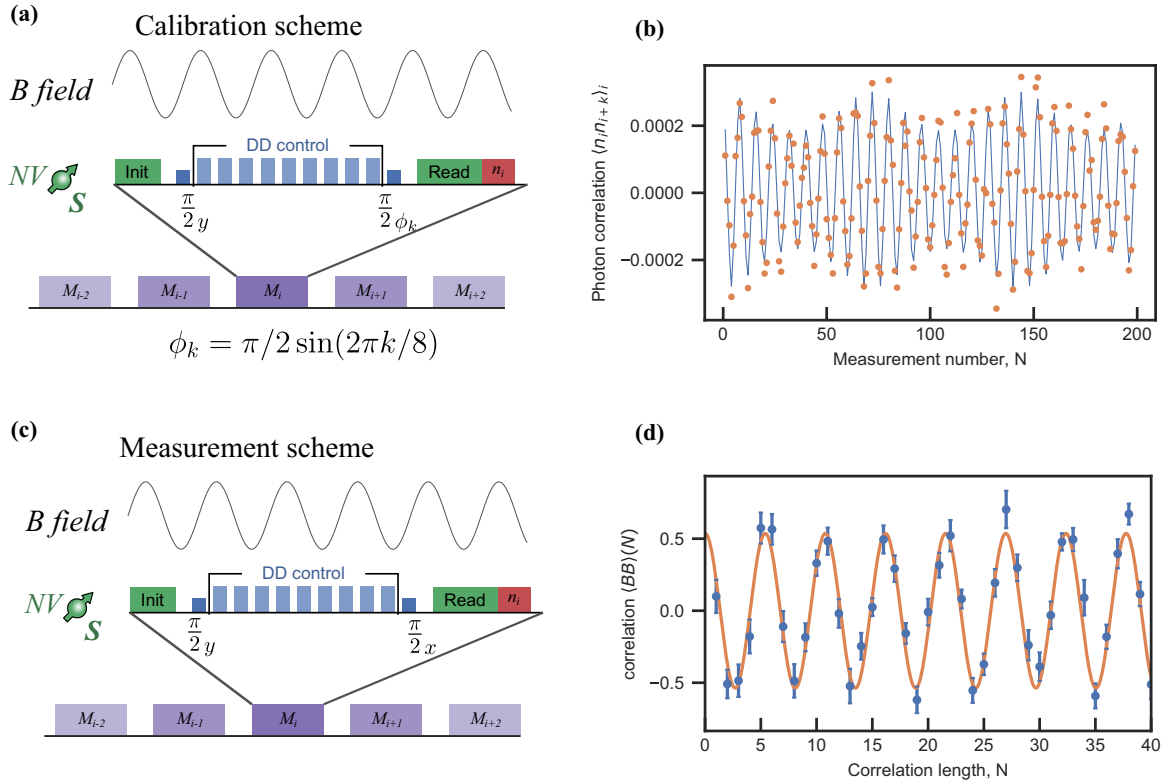
FIG. 2. Externally applied classical field and calibration of fluorescence readout. (a) Experimental protocol for modulation assisted method for determining the fluorescence response of the NV spin readout n_a and n_b. Sequential measurements with optical readout of the electron spin yield phase information obtained by the interaction with the external signal. The readout $\pi/2$ pulse phase is sinusoidally modulated with an amplitude of $\pi/2$ and a period of eight measurement cycles. (b) The empirically calculated correlation of the centered photon count number trace. The beating in the correlation originates from the presence of two frequencies. The size of the beating is determined by the relative amplitude of the external signal to phase modulation. The solid curve is the best fit of the analytical model of the correlation function (2.16), which includes phase modulation and the unknown external signal. (c) Measurement protocol for the estimation of the classical signal correlation function. (d) Reconstructed correlation function of the classical sinusoidal signal with a stochastic phase.

signal into the classical stochastic process of the measured signal.

In Sec. III B a recurrent equation for the dynamics of a composite system (3.51) and the recurrent formula (3.45) for the state of the target nuclear spin are obtained. Under natural assumptions, we get approximate formulas specifying the values of the amplitudes of the observables I_x and I_y corresponding to the nuclear spin at an arbitrary instant of time.

The expression for the amplitude x_N of the I_x component, taking into account incomplete polarization with an indefinite sign, can be represented as [see (3.64)]

$$x_N^\pm \approx \pm \sin \alpha \cos(\omega N t_f) \exp\left[-\frac{(N-1)\alpha^2}{4}\right]$$

$$\approx \pm \sin \alpha \cos(\omega N t_f) e^{-N\Gamma_\perp t_s}, \qquad (2.8)$$

where t_s is the total measurement sequence time [see Fig. 1(a)] and $\Gamma_\perp = \alpha^2/4t_s$ is the measurement-induced dephasing rate. This formula is then used (see Sec. III E) to theoretically calculate the correlation functions [see (3.75)]

$$C^{I_x}(N) = \cos(\omega N t_f) \exp\left[-\frac{(N-1)\alpha^2}{4}\right], \qquad (2.9)$$

for the quantum process corresponding to the component I_x and the classical output process of the component S_z

$$C^{S_z}(N) = \sin^2 \alpha \cos(\omega N t_f) \exp\left[-\frac{(N-1)\alpha^2}{4}\right]$$

$$= \sin^2 \alpha \, C^{I_x}(N). \qquad (2.10)$$

First, we note that formulas (2.9) and (2.10) differ by the factor $\sin^2 \alpha$ in which one $\sin \alpha$ is generated by incomplete polarization (see Sec. III D), and the second $\sin \alpha$ is given by the measurement process itself, while both are determined by the strength parameter α of the weak measurements. Further, although the correlation function $C^{I_x}(N)$ corresponds to the quantum process of the I_x component and its formula includes a pure component $\cos(\omega N t_f)$ corresponding to the Larmor precession, this pure component is distorted by the exponential decay factor.

The above analysis shows that the application of the L-G test to the correlation functions of the output process does not make sense, since this test is designed for noninvasive measurements of the observable in the pure state. However, we can use the theoretical analysis to reconstruct the correlation function of the Larmor precession from experimental data. To do this, we need to be able to restore the parameter α with
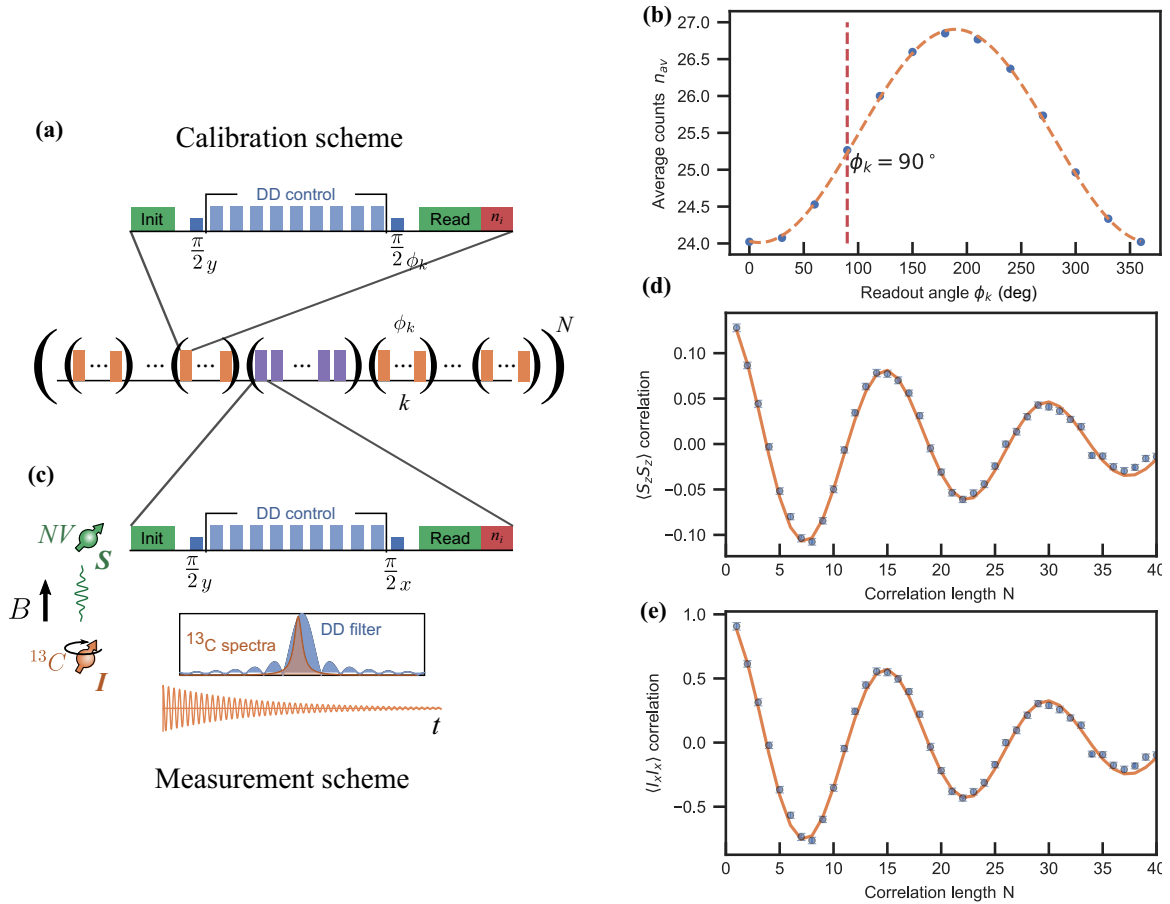
FIG. 3. Reconstruction of quantum correlation function and calibration of fluorescence readout. (a) Experimental protocol for the modulation-assisted method for determining fluorescence response of NV spin readout n_a and n_b. Sequential measurements with optical readout of electron spin results in idle measurements as the DD filter function is detuned from ^{13}C Larmor frequency. The readout $\pi/2$ pulse phase is sinusoidally modulated with amplitude $\pi/2$ and a period of eight measurement cycles. (b) Calibration of n_a and n_b for optical spin readout of the NV center electron spin. The dependence of average photon counts on angle ϕ_k reveals the n_a and n_b photon counts. The model analytical curve [see (2.19)] shows that the response of the NV center depends on n_a and n_b. Measurement scheme [Fig. 3(a)] operates at $\phi_k = 90$. (c) Measurement scheme of the nuclear spin correlation function, operating at $\phi_k = 90$. (d) Empirically estimated correlation of sensor outputs. The solid curve is the best fit of the analytical model for the correlation function, which includes back-action-induced decay of the initial amplitude accounting for a single unknown parameter α. (e) Reconstructed correlation function of the quantum signal.

great accuracy. In the following Secs. II F and II G and in Appendixes F, H, L, we describe the procedures for estimating the parameter α in various experimental modes.

Thus, we come to a simple algorithm for analyzing the experimental data: (1) calculate the empirical correlation function of the classical output signal, (2) normalize the calculated empirical correlation function by $\sin^2 \alpha$ and by exponential decay determined by the measurement-induced dephasing rate $\Gamma_\perp$, and (3) apply the Leggett-Garg inequality to the corrected empirical correlation function.

F. Test experiment with a classical signal

First, we apply these ideas to design of a test experiment in which the NV center interacts not with the nuclear spin, but with an external classical sinusoidal magnetic field with a random phase. The experiment consists of a series of measurements of a classical external oscillating (linearly polarized)

magnetic field [see Figs. 2(a) and 2(c)]

$$B_{ac}(t) = B_{ac} \sin(\omega_{ac} t + \phi), \qquad (2.11)$$

where B_{ac} is the amplitude of the magnetic field $\omega_{ac} = 2\pi f_{ac}$ is the frequency and ϕ is a random phase, using the NV center as a meter. Since the time interval between M_i is not precisely controlled, it can be assumed that each run corresponds to a different realization of the random phase ϕ between the oscillating field and the measurement.

The analysis of the experiment with the classical random magnetic field (2.11) basically follows the approach described above, with some natural modifications. In this experiment, the effective Hamiltonian is given by

$$H_{\text{eff}} = 2\alpha S_z \sin(\omega t + \phi). \qquad (2.12)$$

We can interpret this Hamiltonian as describing the interaction of the NV sensor with a random sinusoidal signal (2.11), where $\alpha = B_z N_p \tau / \pi$ determines the strength of the interaction.
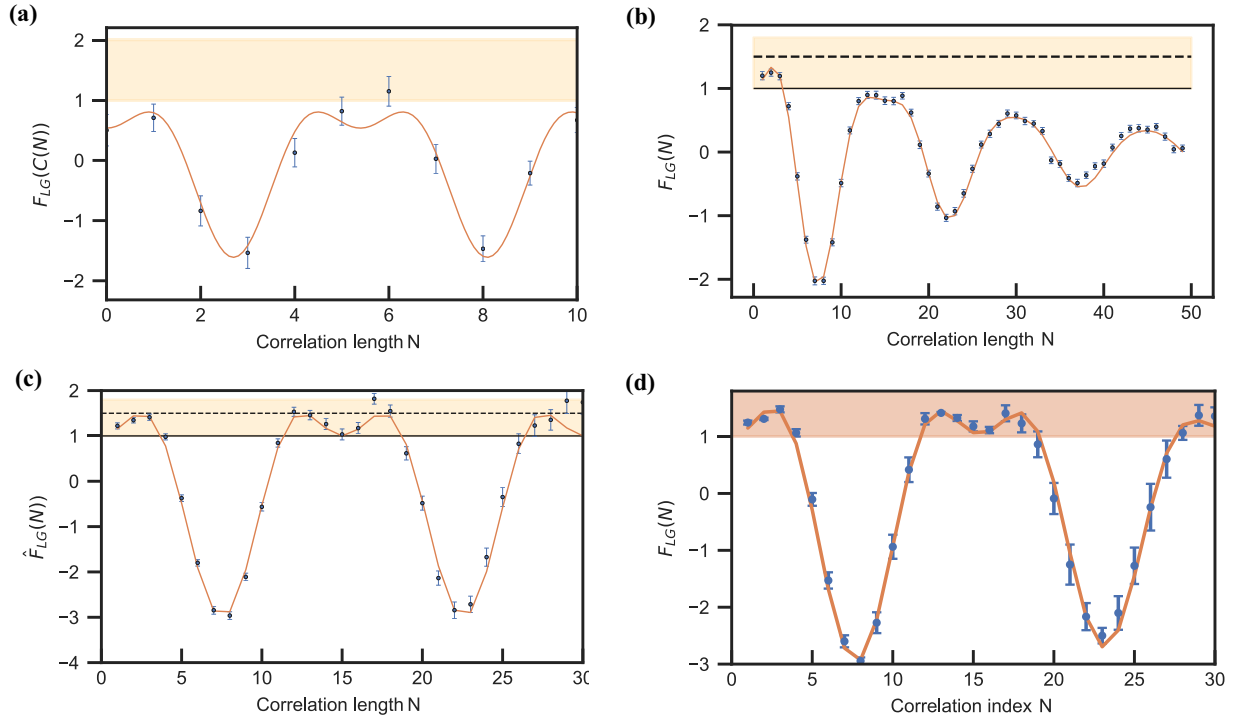
FIG. 4. L-G functions for the classical and quantum processes. (a) L-G function for the reconstructed autocorrelation of the classical r.f. signal. (b) NV2 measurements, L-G function for empirical autocorrelations normalized only by $\sin^2 \alpha$. (c) NV2 measurements, L-G function for empirical autocorrelations normalized by $\sin^2 \alpha$, and dephasing factor. (d) NV2 measurements, the result of averaging L-D functions over five experiments with different control sequences.

Using our theoretical approach, we calculate that the output process is given by

$$z(t) = \pm \sin[\alpha \sin(\omega t + \phi)] \approx \pm \alpha \sin(\omega t + \phi), \quad (2.13)$$

where the approximate equality holds assuming small α. Therefore, the correlation function of the output process $z(t)$ has the following form:

$$\langle z(t)z(t+\tau) \rangle = \frac{\alpha^2}{2} \cos(\omega \tau). \quad (2.14)$$

Recall that the autocorrelation function of the classical random process $x(t) = \sin(\omega t + \phi)$ with a random phase ϕ uniformly distributed on the interval $[0, 2\pi]$ is given by

$$C(\tau) = \frac{1}{2} \cos(\omega \tau). \quad (2.15)$$

Comparing expressions (2.15) and (2.14), we find that they differ only in the factor α^2, which we must extract from a separate experiment.

The result of measurements in our experiment is a sequence $\{n_k\}$ of the number of photons recorded during each readout. Thus, we need to find how the probabilistic properties of counting statistics $\{n_k\}$ are related to the probabilistic characteristics of the sensor signal. We calibrate the fluorescence output n_a and n_b of the NV center for electron spin in the bright $m_s = 0$ and dark $m_s = -1$ states (see Appendix H).

To estimate parameter α a phase modulation

$$\phi_k = \pi/2 \sin(2\pi k/8)$$

is additionally applied to the final $(\pi/2)$ pulse, which modulates the output signal [see Fig. 2(a)]. The empirical correlation function of the output signal has the form [Fig. 2(b)], which is the result of the superposition of the external classical field and the final modulation impulse $\pi/2$. We fit the curve with least-squares method using an analytical expression:

$$\min_{n_a, n_b, \alpha} \sum_{k=1}^{200} \left((\langle n_i n_{i+k} \rangle_i - n_{av}^2) - \frac{(n_a - n_b)^2}{4} \langle S_z^i(\alpha, \Phi_s) S_z^{i+k}(\alpha, \Phi_s) \rangle_i \right)^2. \quad (2.16)$$

Here $n_{av} = (n_a + n_b)/2$ and $S_z^i(\alpha, \Phi_s)$ is the amplitude of the component S_z of the density matrix of the NV spin. As shown in Appendix H, it takes the form

$$S_z^i(\alpha, \Phi_s) = \sin\left[\frac{\pi}{2} \sin\left(\frac{2\pi k}{8} \right) + \alpha \cos\left(\frac{k \Phi_s \pi}{4} \right) \right], \quad (2.17)$$

where Φ [see Appendix H, Eq. (H3)] is the phase acquired under the influence of the DD sequence. As a result, we extract both the fluorescent responses of the NV center in $m_s = 0$ (n_a), $m_s = -1$ (n_b) and the local strength of the RF field (for details see Appendix H). Finally, performing an experimental series without phase modulation, we reconstruct the normalized correlation function of the classical signal [see Fig. 2(d)], using

$$\langle z_i z_{i+k} \rangle_{\text{emp}} = 4 \frac{\langle n_i n_{i+k} \rangle - n_{av}^2}{(n_a - n_b)^2} \qquad (2.18)$$

and Eq. (2.14). Note that the restored correlation function of the classical signal is equal to the analytically calculated function.

G. Calibration of electronic and nuclear spin parameters

To calibrate the fluorescence output n_a and n_b of the NV center for electron spin in the bright $m_s = 0$ and dark $m_s = -1$ state, we apply a phase modulation to the final $(\pi/2)$ pulse [see Fig. 3(a)]. In a series-averaged output, we obtain an oscillating signal, which is fitted with

$$n(k) = \tfrac{1}{2}(n_a + n_b) + \tfrac{1}{2}(n_a - n_b)\sin^2(\phi_k/2 + \phi_0), \quad (2.19)$$

where ϕ_k are the modulation angles in series $0, 30, 60, 90, \ldots, 360$, n_a and n_b are bright and dark photon count rates [see Fig. 3(b)]. The $\phi_0 \ll 1$ is the phase offset due to imperfections of the pulses due to detuning. The measurement scheme [Fig. 3(a)] operates at $\phi_k = 90$. Each angle series consists of 50 sequential measurement, and $\phi_k = 90$ is measured 500 times [see Fig. 3(a), number of measurements in inner brackets].

Then we calculate the empirical correlation function for the registered photons using the formula

$$C_n(N) = \langle n_i n_{i+N} \rangle = \frac{1}{k-N} \sum_i^k n_i n_{i+N}$$

and the empirical electron spin correlation

$$C_{S_z}(N) = \frac{4[C_n(N) - n_{av}^2]}{(n_a - n_b)^2} \qquad (2.20)$$

using the estimated parameters n_a and n_b from Fig 3(b). We evaluate the parameters α, using the standard least-squares method ($\phi = \omega t_f$) by comparing the empirically estimated $C_{S_z}(N)$ to the analytical one [Eq. (2.10)]. In this way we find an estimate of α with which Eq. (2.10) approximates the reconstructed correlation function of the output signal in an optimal way [see Fig. 3(c)]. After carefully measuring the calibration constant α we normalized the empirical correlation function $C_{S_z}(N)$ by $\sin^2 \alpha$ and get an estimation of $C_{I_x}(N)$ [see Fig. 3(d)].

H. Main results

We use the Leggett-Garg (L-G) test in the following form (see, e.g., [26]):

$$\text{LG}(\tau) = 2C(\tau) - C(2\tau). \qquad (2.21)$$

Let us first consider the case of a classical input sinusoidal signal with a random phase. In Fig. 4(a) it can be seen that even after correcting the empirical correlation function by the factor α^2, as expected, there is no violation of the L-G inequality.

In the case of measurement of the nuclear spin NV2, we first consider the case when the empirical correlation function is corrected only on the factor $\sin^2 \alpha$ [see Fig. 4(b)]. In this case the inequality is violated until the damping effect manifests itself, that is, only at several initial points, the number of which depends on the parameter α. The demonstrated result corresponds to the following experimental parameters: KDD-XY5 sequence, free precession angle $\approx 27°$, polarized ^{14}N, and $\alpha \approx 0.18\pi$. In this case decoherence is fast, and we recognize only three points of disturbance and only in the first period of oscillation.

Figure 4(c) shows the case where the empirical correlation function is corrected by an exponential decay factor. It is noteworthy that with such a correction, the correlation function demonstrates a violation of inequality in the second and even third fluctuations. In total, we conducted five experiments. We used a simplified version of memory-enhanced readout proposed in [22], where the NV electron spin is mapped to ^{14}N. We performed 200 repetitive readouts per single measurement and calculated the resulting number of photons instead of using the maximum likelihood method. Figure 4(d) shows the result of the result of averaging over five experiments with different control sequences. Again, the correlation function demonstrates a reliable violation of the inequality in the third oscillation.

Finally, we discuss the effects of ionization on the recorded data. It was found that the NV center is in the dark state during green excitation for $\approx 30\%$ of the time without an observable fluorescence fingerprint. Ionization of the NV center has been identified as the limiting decoherence mechanism for quantum memories used for long-range quantum communication optical networks. However, as we emphasized above, the values of the signal in the initial period, when the back-action does not yet distort the signal, are fundamentally important for our experiment. Therefore, we select control actions that are aimed not at achieving the longest oscillation duration, but at the least signal distortion in the initial period. We simulate the process of sequential weak measurements with initially polarized target spin using the Monte Carlo method and conclude that the errors induced by the charge state are less than statistical errors and do not affect our final conclusions. A more detailed ionization mechanism and the results of numerical simulations are given in Appendix E.

In conclusion, we showed that the empirical correlation functions corrected on the basis of our theoretical model do break the LG inequality in different measurement regimes. We also showed that in a test experiment with an input random classical signal, the empirical correlation function corrected in accordance with the theory does not violate the inequality. These results allows us to conclude that, first, our model and theoretical analysis describe the experiment quite well, and second, that the strength parameter α of weak measurements is estimated experimentally with high accuracy. This means that we correctly reconstruct the correlation of the quantum Larmor precession, which, of course, violates the LG inequality according to the theory. The above results show that although we cannot avoid the inevitable decoherence effect

during the measurement process, we can account for these changes based on theoretical analysis and accurate empirical reconstruction of the experimental parameters.

We also note that in the process of analysis, we restore the sequence of transformations of the initial state from a purely quantum state to a classical macroscopic state at the output of the system (see Sec. III).

III. THEORETICAL ANALYSIS OF EXPERIMENT

A. Notation and preliminaries

The process of repeated (weak) measurements of some quantum observable is implemented on the composite Hilbert space $\mathcal{H} = \mathcal{H}_D \otimes \mathcal{H}_Q$ by coupling the primary quantum system Q, initially in the ρ state, on the Hilbert space $\mathcal{H}_Q$, to a quantum measuring device D, initially in the state σ. The two systems interact during a period τ, and after interaction, the initial density matrix is transformed into

$$\rho_{QD}(\tau) = U(\tau)\rho \otimes \sigma U^*(\tau), \qquad (3.1)$$

where U is a unitary operator acting on the composite system. The unitary group $U(\mathcal{H})$ consists of complex linear operators U on $\mathcal{H}$, which satisfy $UU^* = \mathbb{1}$, and, accordingly, the Lie algebra $\mathfrak{u}(\mathcal{H})$ of this group consists of anti-Hermitian operators.

The manifold of general quantum states is the family of orbits of the smooth action of the group $GL(\mathcal{H})$ of invertible operators on $\mathcal{H}$ acting on the space of self-adjoint operators according to the map [31]

$$\mathfrak{u}^*(\mathcal{H}) \ni A = A^* \to gAg^*, \quad g \in GL(\mathcal{H}). \qquad (3.2)$$

In this picture, pure states form an orbit in the dual space $\mathfrak{u}^*(\mathcal{H})$. This action does not preserve the spectrum and the trace of A unless g is unitary; however, it preserves the positivity of A and *the rank of A.*

In the case of a composite 2×2 system (in particular, two spin system $S = 1/2$ and $I = 1/2$), the basis of the state space can be written as the direct product of the basis sets of the single spins

$$\{S_e, S_x, S_y, S_z\} \otimes \{I_e, I_x, I_y, I_z\}, \qquad (3.3)$$

where $S_e = I_e = \frac{1}{2}\mathbb{1}$, $I_i = \frac{1}{2}\sigma_i$. In this case the local transformations of density matrices form a six-dimensional subgroup $SU(2) \otimes SU(2)$ of the full unitary group $U(4)$. For an isolated system with dynamical symmetry group $SU(2)$ there exists the corresponding (real) Lie algebra $\mathfrak{su}(2)$, spanned by the operators $\{iI_x, iI_y, iI_z\}$ satisfying the angular momentum commutation relations

$$[I_x, I_y] = iI_z \qquad (3.4)$$

and cyclic permutations, where $I_i = \frac{1}{2}\sigma_i$ and σ_i, $i = x, y, z$ are Pauli matrices. So the pure state can be expressed in terms of the basis of observables and identified with a point on the surface of the Bloch ball as the Bloch vector

$$\rho = I_e + xI_x + yI_y + zI_z := \mathbf{w} \cdot \mathbf{I},$$
$$x = \mathrm{tr}[\rho\,\sigma_x], \quad y = \mathrm{tr}[\rho\,\sigma_y], \quad z = \mathrm{tr}[\rho\,\sigma_z],$$
$$\mathbf{w} = (x, y, z), \quad \mathrm{tr}[\rho] = \mathrm{tr}[\rho^2] = 1. \qquad (3.5)$$

The mixed states correspond to the points inside the Bloch ball $|\mathbf{w}| = \mathrm{tr}[\rho^2] < 1$. Unitary operations can be interpreted as rotations of the Bloch ball and the dissipative processes as linear or affine contractions of this ball.

It is generally considered that a quantum-mechanical system which is isolated from the external world has a Hamiltonian evolution. If $\mathcal{H}$ is the Hilbert space of the system, this is expressed by the existence of a self-adjoint (Hamiltonian) operator H, such that the state ρ at time t is computed from the state at time 0 according to the law $\rho_t = e^{-itH}\rho e^{itH}$. A *composite* system represented in terms of a Lie group can be considered as isolated from the environment.

To analyze the impact of a unitary group on the state of the system we can use the Baker-Campbell-Hausdorff (BCH) formula. The BCH formula reveals the formal purely algebraic connection between the local structure of a Lie group G and its algebra $\mathfrak{g}$. If one makes no further simplifying assumptions, then the BCH formula for the orbit $e^H\rho e^H$ expands to an infinite series of nested commutators. But, in a particular case, under the condition

$$[H, [H, \rho]] = \rho$$

(for example, $[S_i, [S_i, S_j]] = S_i$ if $S_i \neq S_j$,) the exact formula holds:

$$e^{-i\phi H}\rho e^{i\phi H} = \rho \cos\phi - i[H, \rho]\sin\phi. \qquad (3.6)$$

This means that if the experiment is constructed so that the interaction Hamiltonian is expressed in terms of some basis operator S_i, then the dynamics of the object can be calculated using (3.6). However, the formula (3.6) does not work in the case when, as a result of interactions, the system passes into an entangled state, which is necessary to obtain information about the measurement object.

A state ρ_{QD} of a composite quantum system is called *entangled* if it cannot be represented as a convex combination

$$\rho_{QD} = \sum_\alpha p_\alpha \rho_\alpha^1 \otimes \rho_\alpha^2, \quad \text{with} \quad \sum_\alpha p_\alpha = 1, \qquad (3.7)$$

where ρ_α^1, ρ_α^2 are density matrices of the two subsystems. Recall that a bipartite pure state ρ_{QD} *is entangled* if and only if its reduced states are *mixed states*. (Moreover, a pure state of a composite system is entangled if and only if it violates Bell's inequality [32]; however, the assumption that violation of some Bell inequality is equivalent to the concept of entanglement is incorrect [33,34].)

In our case, *entanglement* manifests itself in the appearance of zero commutators in the BCH expansion of the composite system, such as (3.19).

The local properties *of mixed states* of two subsystems of an entangled composite system can be studied by analyzing the *action* of the elements of the local subgroup $Loc = SU(2) \otimes SU(2)$ of the group $U(4)$ on state ρ of a composite system lying in orbit

$$\{\rho' = U\rho U^*, \ U \in SU(2) \otimes SU(2)\}. \qquad (3.8)$$

For this purpose, the real symmetric 6×6 Gram matrix is introduced:

$$G_{ij} := \tfrac{1}{2}\mathrm{tr}(W_i W_j), \quad W_j := [R_j, \rho], \quad j = 1, \ldots, 6,$$
$$R_k = i\sigma_k \otimes \mathbb{1}_2, \quad R_{k+3} = \mathbb{1}_2 \otimes i\sigma_k, \quad k = 1, 2, 3, \tag{3.9}$$

where the anti-Hermitian matrices R_i, $i = 1, \ldots, 6$, form a basis of the $\mathfrak{su}(2) \oplus \mathfrak{su}(2)$ Lie algebra. It turns out [35], that the *rank* of the Gram matrix is a *geometric invariant* [cf. the mapping (3.2)] of the orthogonal transformations, which does not change along the orbit (3.8). Since a state ρ_{QD} of the composite system is expressed in terms of Pauli matrices, the commutators $[R_j, \rho]$ can also be represented in terms of $[\sigma_k \otimes \mathbb{1}, \sigma_j \otimes \mathbb{1}]$. Therefore, if the interaction Hamiltonian H applied to a composite system in a separable state ρ_{QD} generates zero terms [see (3.19)]

$$[\sigma_k \otimes \mathbb{1}, \sigma_j \otimes \mathbb{1}] = 0$$

in the BCH formula, it can serve as *evidence of the transition* of a separable state to an entangled one. The degeneracy of the Gram matrix and, as a consequence, the appearance of zero terms violate the conditions for the applicability of formula (3.6).

Despite this, in our simple model, we can derive a modified exact BCH formula (see Appendix B). If the conditions

$$B = [H, \rho], \quad [H, B] = k\rho - k\Delta, \tag{3.10}$$

$$[H, \Delta] = 0 \quad [H, [H, B] + k\Delta] = [H, [H, B]]. \tag{3.11}$$

are met, the following modification of the BCH formula holds:

$$U \rho U^* = e^{-iH\phi} \rho e^{iH\phi} = \rho \cos(\phi\sqrt{k}) + \Delta[1 - \cos(\phi\sqrt{k})]$$
$$- \frac{1}{\sqrt{k}} i[H, \rho] \sin(\phi\sqrt{k}). \tag{3.12}$$

POV measures naturally arise in the process of repeated measurements of a quantum observable. The POVM method is a realization of Naimark's theorem (see, e.g., [36–38]), which states roughly that the POVM scheme is equivalent to projective measurements in an extended Hilbert space (the von Neumann–Lüder projection measurements). The discrepancy between the original and extended Hilbert spaces is interpreted as the presence of perturbations or inaccuracies in measurements (see Appendix C).

Completely positive, trace-preserving maps arise in the POVM measurement scheme, when one wishes to restrict attention to a subsystem $\mathrm{U}(\mathcal{H}_Q)$ of a larger system $\mathrm{U}(\mathcal{H}_D) \otimes \mathrm{U}(\mathcal{H}_Q)$. The postmeasurement state ρ_Q of the *primary system* Q is obtained by projecting the joint state ρ_{QD} of the entangled system QD into the subspace of quantum subsystem by taking a *partial trace* with respect to the ancilla.

The basic characterization of the measurement model is given by the quantum operation S_α [see (C6) in Appendix C], which is the linear transformation of the initial state corresponding to a projection measurement given by an orthogonal projector P_α. The postmeasurement state of the *primary system* is obtained by taking a partial trace (C4) with respect to quantum measuring device D. Thus, the map S_α must at least be both *trace-preserving* and *positive-preserving* in order to preserve the density matrix property. However, the latter is not sufficient, since S_α must be the result of a *positivity-preserving*

process on the larger system $U(\mathcal{H}_D) \otimes U(\mathcal{H}_Q)$ of operators, which is essentially an informally definition of *the complete positivity* of S_α. Every completely positive map S_α can be represented (nonuniquely) in the Kraus form [37],

$$S_\alpha(\rho) = \sum_k \left(M_k^\alpha\right)^* \rho M_k^\alpha, \tag{3.13}$$

with some set of operators M_k^α. The probability to obtain result α in the measurement is given by [see (C10) for details]

$$\mathbb{P}_{\rho \otimes \sigma}(\alpha) = \mathrm{tr}\left[\rho \sum_k \left(M_k^\alpha\right)^* M_k^\alpha\right] := \mathrm{tr}[\rho F_\alpha], \tag{3.14}$$

where [see (C8)]

$$F_\alpha = \sum_k \left(M_k^\alpha\right)^* M_k^\alpha = \mathrm{tr}_D[U^* P_\alpha U \sigma]. \tag{3.15}$$

Therefore, we may identify a set of Kraus operators $\{M_k^\alpha\}$ or, equivalently, a set of effects $\{F_\alpha\}$ with a generalized observable defined by a *positive operator-valued measure*

$$R(E) = \sum_{\alpha \in E} F_\alpha, \quad E \subset \mathbb{Z}.$$

Equation (3.15) demonstrates that a physical quantity F_α of a physical system is actually identified by the real experimental equipment used to measure it. Thus, quantum observables, defined by $\{F_\alpha\}$ and measured relative to a reference frame (ancillas), can be considered as relative attributes.

The representation (3.14), which is the result of a inverse mapping of the detector output to the target system, allows us to introduce an analog of the classical *relative entropy* of Kullback and Leibler as a measure of the discrepancy of information that occurs during the measurement process [see definition (C12) and discussion in Appendix C, and application in (III E)].

A sequence of (weak) POVM measurements given by a completely positive stochastic map $S(\rho)$ generates a set of orbits inside the Bloch ball. Each measurement reduces the parameters of orbits, and a sequence of measurements produces an inward-spiraling precession, which sequentially traverses the orbits.

The stratification of the Bloch ball by the orbits can be considered as a *natural quantization* generated by POVM measurements.

B. Interaction in the *x-y* plane

The simple basic idea of the experiment is to study the precession of a spin-$\tfrac{1}{2}$ particle under the action of the Hamiltonian $H = -\omega I_z$ with some angular precession frequency ω. The nuclear spin undergoes a free precession around the z axis with an angular velocity given by the Larmor frequency ω. We expect the L-G inequality, which limits the strength of temporal correlations in the classical structure, to be violated by the quantum mechanical unitary dynamics of the Larmor precession. However, in a real experiment, a challenging task is to implement and analyze the measurement procedure, which is carried out using another quantum object as a meter. In this section we will pass through this procedure step by step.

1. Initial condition

We start the analysis of the experiment with the initial condition of the composite system corresponding to the idealized polarized state of the target nucleus spin

$$\rho(0) = \rho^S(0) \otimes \rho^I(0) = (S_e + S_z) \otimes (I_e + I_x). \quad (3.16)$$

In our experiment, we investigated both polarized and unpolarized initial conditions of the nuclear spin. As shown in Sec. III D, an experiment with an unpolarized initial state results in partial polarization during measurements. Note also that prepolarization procedures (see [25,39]) are never 100% efficient. How to take into account the influence of incomplete polarization on the final result is discussed in Sec. III D. We consider an experiment with a polarized initial condition as a basic idealized measurement model.

2. Step 1, substep 1

We consider the transformation of a composite system, which is in the initial state (3.16), under the influence of the Hamiltonian $H = -\omega I_z$, and apply the BCH formula to calculate the result of this transformation

$$\rho_1(1) = (S_e + S_x) \otimes [I_e + I_x \cos(\omega t_f) + I_y \sin(\omega t_f)]. \quad (3.17)$$

Information about the quantum Larmor precession itself arises as amplitudes $x = \cos(\omega t_f)$ and $y = \sin(\omega t_f)$ of the observables I_x and I_y. Since entanglement does not occur under this action, the state of the electron spin does not change.

3. Step 1, substep 2

Next, we study the interaction between the NV sensor and the target nuclear spin in the x-y plane, which under the action of the KDD sequence is determined by the effective Hamiltonian [24,29,30]

$$H_{\text{eff}} = 2\alpha S_z \otimes I_x. \quad (3.18)$$

The influence of the KDD sequence is specified by the measurement strength parameter α, which depends on the perpendicular component $A_\perp$ of the hyperfine field and can be controlled by the number and duty cycle of pulses (see Sec. II). To study evolution, we apply the propagator $\exp(-2\alpha S_z \otimes I_z)$ to the density matrix (3.17).

Before applying the BCH formula, we calculate the commutator $[H, \rho]$:

$$[H, \rho] = [2\alpha S_z \otimes I_x, (S_e + S_x) \otimes (I_e + xI_x + yI_y)]$$
$$= [2\alpha S_z \otimes I_x, S_e \otimes (I_e + xI_x)] + [2\alpha S_z \otimes I_x, S_e \otimes yI_y]$$
$$+ [2\alpha S_z \otimes I_x, S_x \otimes I_e + xI_x]$$
$$+ [2\alpha S_z \otimes I_x, S_x \otimes I_e + xI_x].$$

Notice that

$$[S_z \otimes I_x, S_x \otimes I_y] = 0, \quad (3.19)$$

$$[S_z \otimes I_x, S_e \otimes (I_e + xI_x)] = [S_z, S_e] \otimes \tfrac{1}{2}(I_x + xI_e) = 0, \quad (3.20)$$

which indicates the transition of a separable state (3.17) into an entangled state as a result of interaction (see Sec. III A).

Hence,

$$B := [H, \rho] = [2\alpha S_z \otimes I_x, S_e \otimes yI_y]$$
$$+ [2\alpha S_z \otimes I_x, S_x \otimes I_e + xI_x]$$
$$= i\frac{1}{2}S_y \otimes (xI_e + I_x) + \frac{i}{2}S_z \otimes yI_z \quad (3.21)$$

and

$$[H, B] = k\Delta + k\rho, \quad \sqrt{k} = 1/2, \quad (3.22)$$

$$\Delta = (S_x \otimes yI_y) + S_e \otimes (I_e + xI_x). \quad (3.23)$$

Thus, applying the BCH formula (3.12) we get

$$\rho_2(1) = (\cos \alpha)\rho^S \otimes \rho^I \quad (3.24)$$
$$- \frac{i}{1/2}\sin\alpha\left[\frac{i}{2}S_y \otimes (xI_e + I_x) + \frac{i}{2}S_z \otimes yI_z\right] \quad (3.25)$$
$$= (\sin\alpha)S_y \otimes (xI_e + I_x) \quad (3.26)$$
$$+ S_e \otimes (I_e + xI_x) + (\cos\alpha)S_e \otimes yI_y \quad (3.27)$$
$$+ (\sin\alpha)S_z \otimes yI_z \quad (3.28)$$
$$+ (\cos\alpha)S_x \otimes (I_e + xI_x) + S_x \otimes yI_y, \quad (3.29)$$

which already clearly shows that entanglement has occurred. We note that a similar expression is given in [25]; however, it remained unclear for us how it was obtained.

This result immediately leads to *a postinteraction estimation* of the state of the nuclear spin. Following the POVM analysis rules (see Appendix C), we estimate the new state $\rho_2^I(1)$ of the nuclear spin by taking the *partial traces* over the NV sensor and the state of NV spin $\rho_2^S(1)$, respectively:

$$\rho_2^I(1) := \text{tr}_S[\rho_2(1)] = I_e + I_x \cos(\omega t_f) + I_y \sin(\omega t_f)\cos\alpha, \quad (3.30)$$

$$\rho_2^S(1) := \text{tr}_I[\rho_2(1)] = S_e + S_x \cos\alpha + S_y \cos(\omega t_f)\sin\alpha. \quad (3.31)$$

Note also that as a result of the interaction, the coordinate x of the observable I_x is mapped into the coordinate $\theta = \cos(\omega t_f)\sin\alpha$ of the observable S_y of the NV sensor with the factor $\sin\alpha$, which specifies the magnitude of the measurement and, as a consequence, the *incompleteness* of the information obtained during the weak measurement.

4. Step 1, substep 3

The rotation of the electronic spin is performed by applying $\pi/2$ pulse along S_x:

$$\rho_3(1) = (\sin\alpha)S_z \otimes (xI_e + I_x) \quad (3.32)$$
$$+ S_e \otimes (I_e + xI_x) + (\cos\alpha)S_e \otimes yI_y \quad (3.33)$$
$$- (\sin\alpha)S_y \otimes yI_z \quad (3.34)$$
$$+ (\cos\alpha)S_x \otimes (I_e + xI_x) + S_x \otimes yI_y. \quad (3.35)$$

Again, by taking the *partial traces* over the NV sensor and nuclear spin we obtain

$$\rho_3^I(1) := \mathrm{tr}_S[\rho_3(1)] = I_e + I_x \cos(\omega t_f) + I_y \sin(\omega t_f) \cos\alpha,$$
(3.36)

$$\rho_3^S(1) := \mathrm{tr}_I[\rho_3(1)] = S_e + S_x \cos\alpha + S_z \cos(\omega t_f) \sin\alpha.$$
(3.37)

Thus, the rotation of the electron spin leads to a mapping of the S_y coordinate of the NV sensor and, consequently, the x amplitude of the nuclear component I_x onto the amplitude of the optically readable S_z component of the NV sensor given by

$$\zeta_1 := \mathrm{tr}\big[\sigma_z \rho_3^S(1)\big] = x \sin\alpha = \cos(\omega t_f) \sin\alpha.$$

5. Step 1, substep 4

The final projective measurement along the z axis is the *optical readout* of the observable S_z with eigenvalues and corresponding projection operators given by the formula

$$\lambda_+ = \tfrac{1}{2}, \quad \lambda_- = -\tfrac{1}{2},$$
$$S^\alpha = S_e + S_z, \quad S^\beta = S_e - S_z$$
(3.38)

These measurements are defined by the probabilities

$$\mathbb{P}(\lambda_+) = \mathrm{tr}[\rho_3^S(1) S^\alpha] \quad \text{and} \quad \mathbb{P}(\lambda_-) = \mathrm{tr}[\rho_3^S(1) S^\beta].$$
(3.39)

Remark III.1. Canonical projective measurement is usually viewed as an instantaneous act or spontaneous collapse of the probability amplitude. However, the optical projective measurement is a quantum stochastic (nonunitary) process, which has been intensively studied from both a physical and mathematical point of view (see, e.g., [36,40]). We postpone the discussion of this problem to Sec. III C and Appendix D.

An optical readout repolarizes the sensor back on to the initial state $\rho^S(0) = (S_e + S_z)$, while leaving the nuclear spin in the x-y plane, so in the next cycle of measurements we start with the next free precession applied to the state

$$\rho^S(0) \otimes \rho_3^I(1) = (S_e + S_z) \otimes [I_e + I_x \cos(\omega t_f)$$
$$+ I_y \sin(\omega t_f) \cos\alpha].$$

By repeating the above measurement process, we obtain after N measurements

$$\rho^I(N) = I_e + x_N I_x + y_N I_y,$$
(3.40)

$$\rho^S(N) = S_e + \xi_N S_x + \theta_N S_y + \zeta_N S_z,$$
(3.41)

where coordinates x_N and y_N are given by the recurrent equations

$$x_N = x_{N-1} \cos(\omega t_f) - y_{N-1} \sin(\omega t_f),$$
(3.42)

$$y_N = x_{N-1} \sin(\omega t_f) \cos\alpha + y_{N-1} \cos(\omega t_f) \cos\alpha,$$
(3.43)

with $x_0 = 1$ and $y_0 = 0$. The recorded output amplitude ζ_N is given by

$$\zeta_N = \mathrm{tr}[\sigma_z \rho^S(N)] = x_N \sin\alpha.$$
(3.44)

In terms of Bloch vectors $\vec{\rho} = (x, y, z)$, the system of Eqs. (3.42) and (3.43) can be written as follows:

$$\vec{\rho}_I(N) = \mathcal{R}_z^\alpha \vec{\rho}_I(N-1),$$
(3.45)

where the operator $\mathcal{R}_z^\alpha$ is given by

$$\begin{bmatrix} \cos(\omega t_f) & -\sin(\omega t_f) & 0 \\ \sin(\omega t_f)\cos\alpha & \cos(\omega t_f)\cos\alpha & 0 \\ 0 & 0 & 1 \end{bmatrix}.$$
(3.46)

For a sufficiently small α, by the same reasoning as in [25], one can obtain from (3.42) and (3.43) the following approximate representation of the dissipative process:

$$x_N \approx \cos(\omega N t_f)(\cos(\alpha/2))^{2(N-1)},$$
(3.47)

$$\approx \cos(\omega N t_f) \exp\left[-\frac{(N-1)\alpha^2}{4}\right],$$
(3.48)

$$y_N \approx \sin(\omega N t_f) \cos\alpha [\cos(\alpha/2)]^{2(N-1)},$$
(3.49)

$$\approx \sin(\omega N t_f) \cos\alpha \exp\left[-\frac{(N-1)\alpha^2}{4}\right].$$
(3.50)

This representation corresponds to the well-known form of solutions of the classical Bloch equations for the transverse components M_x, M_y.

Finally we note that with

$$\Delta = \rho - 4[H, [H, \rho]] \quad \text{and} \quad \sqrt{k} = 1/2,$$

the closed form (3.12) of the BCH formula can be rewritten in the form of the master equation

$$\rho_N - \rho_{N-1} = -2i[H, \rho_{N-1}] \sin\alpha$$
$$- 4[H, [H, \rho_{N-1}]](1 - \cos\alpha),$$
(3.51)

where $[H, \rho_{N-1}]$ is the group generator and

$$4[H, [H, \rho_{N-1}]](1 - \cos\alpha)$$

the *damping term* ($\alpha := \phi\sqrt{k}$). In the specific case of our experiment, taking into account (3.23), we can rewrite Eq. (3.51) as follows:

$$\rho_N = -2i[H_{\text{eff}}, \rho_{N-1}] \sin\alpha + \rho_{N-1} \cos\alpha$$
$$+ (S_x \otimes y_{N-1} I_y + S_e \otimes (I_e + x_{N-1} I_x))(1 - \cos\alpha).$$
(3.52)

Note that Eq. (3.52) can be considered as an analog of the qubit master equation in Ref. [41] [Eqs. (3.10) and (3.14)] for the model of measurements in circuit quantum electrodynamics (QED), that is, as a discrete time analog of the master equation in the *Born-Markov approximation in the Lindblad form*. This is not surprising, since the master equations in Refs. [42,43], as well as in other papers, were obtained using perturbation formulas such as the Lie-Trotter formula or Kato's perturbation formula, under some additional strong assumptions. For example, in Refs. [36,44] the Markovian master equations are given under the assumption of the weak coupling limit. In Refs. [42,43] the main postulate besides the Markov property was the *complete positivity* of the generator of the quantum semigroup. This is a strict assumption, the importance of which we discussed in connection with the concepts of entanglement and POVM measurements. Our exact formula, of course, stems from the simplicity of the particular experimental model that allows the closed BCH formula to be used.

C. Optical projective readout

As we mentioned in the Sec. II F, the result of measurements in our experiment is a sequence $\{n_k\}$ of the number of photons recorded during each readout period. Thus, the goal of the theory is to obtain a formula for the probability $\mathbb{P}(m, [0, t))$ that m counts are recorded in the interval $[0, t)$. [How to relate it to the probabilities (3.39) given by the theory is explained in Appendixes H and I; see also [45,46].]

Such formulas were obtained in the 1960s for both classical and quantum optical fields and in the phase space representation ($z = x + iy$) can be formally written in a similar form (see, e.g., [40]):

$$\mathbb{P}(m, [0, t)) = \frac{1}{m!} \int \varphi(z)(|z|^2 \alpha t)^m e^{-|z|^2 \alpha t} \, d^2z, \qquad (3.53)$$

where α characterizes the efficiency of the detector. In this formal connection, the weight function $\varphi(z)$ (called the Wigner quasiprobability distribution, or Glauber P representation) is an analog of the classical distribution function, but, in the general case, it is not nonnegative. (See, e.g., the well-known example of a simple harmonic oscillator introduced by Groenevold [47] in 1946.) Thus, the similarity in form does not mean that the quantum theory is physically equivalent to the classical theory and is called the optical equivalence theorem. In cases where the measurement model leads to a positive normalized function $\varphi(z)$, it becomes a conventional normal distribution function, and formula (3.53) determines a meaningful distribution for all T. There are examples when the negativity of the function φ does not give rise to any difficulties in the analysis if the basic laws of the theory are not violated. However, the question arises when φ is the usual probability density, and, consequently, as a result of measurements, we get a classical stochastic (macroscopic) process.

It follows from the analysis of Sec. III B that, under the influence of a sequence of weak measurements, the state of the target spin tends to a totally mixed state (3.55). Thus, the transformation of a quantum random process into a classical one cannot be explained by decoherence alone. To do this, it is necessary to take into account that the process of projective optical readout is carried out with limited accuracy.

In our experiment the basic photo-physical mechanisms behind the optical detection of the NV spin are well developed (see, e.g., [45,46]). The spin dependence of the fluorescence arises through an intersystem crossing to metastable singlet states, which occurs preferentially from the $m_s = \pm 1$ excited states. The transient fluorescence signal is typically measured by counting photons in a brief period following optical illumination. This inevitable strategy misses part of the signal because the differential fluorescence remains after the time cutoff, while photons arriving near the end of the counting interval are overweight.

The effect of error in an optical (nonunitary) readout process can be described using a variant of the POVM method (see Appendix D), similar to how the occurrence of decoherence as a result of Hamiltonian transformations was demonstrated in Sec. III B. The Wigner distribution $\varphi(z)$ can indeed be negative, but when integrated with a certain nonnegative normalized weight function $\sigma_\alpha(x, y)$ it gives a conventional probability distribution

$$\rho_\alpha(x, y) = \int_{\mathbb{R}^2} \varphi(x - \xi, y - \eta)\sigma_\alpha(\xi, \eta) \, d\xi \, d\eta. \qquad (3.54)$$

Moreover, if this weight function $\sigma_\alpha(x, y)$ depends on a parameter α, which characterizes the measurement error of the detector, then using the POVM method it is possible to show that $\rho_\alpha(x, y)$ corresponds to new *commutative approximate* observables of position and momentum [see (D10) and (D11) in Appendix D]. This is of course consistent with the interpretation that in the case of successive unitary transformations of a composite system, observables F_α given by (3.15) are generated.

The exact meaning of this approach and the mathematical details are explained in Appendix D.

Thus, we may conclude that the transition from a quantum process to a classical one in the optical projective measurement can be explained as a consequence of measurement inaccuracy. This apparently explains the fact that the results of theoretical analysis based on a macroscopic model [48] and the classical probabilistic scheme assuming Poisson statistics and independence of repeated observation bins [46] give a good approximation in the analysis of experimental data.

D. Initial state generation

The special polarization procedure (see [25,39]), does not guarantee 100% polarization. In this regard, below we analyze the process which realizes an incomplete (depending on α) polarization of the nuclear spin during the first few measurements.

In this case, the initial condition is believed to be the thermal equilibrium state which is the result of interactions with other spins and the environment and is described by the totally mixed state

$$\rho_0^I = \tfrac{1}{2}|0\rangle\langle 0| + \tfrac{1}{2}|1\rangle\langle 1| = \tfrac{1}{2}I_\alpha + \tfrac{1}{2}I_\beta = I_e. \qquad (3.55)$$

As for the sensor spin, NV center is easily optically pumped with suitable fidelity into the polarized state $|0\rangle$. Thus, the initial state of the combined system can be naturally assumed to be

$$\rho^0 = \rho_S(0) \otimes \rho_0^I = (S_e + S_z) \otimes I_e. \qquad (3.56)$$

After the $\pi/2$ pulse to NV spin about the y axis this state is converted to

$$\rho_1^0 = (S_e + S_x) \otimes I_e. \qquad (3.57)$$

This state is separable but not absolutely separable [49]; therefore we can get an entangled state with the help of a global transformation. To this end, we first apply the interaction controlled by the Hamiltonian $H_{\text{eff}} = 2\alpha S_z \otimes I_x$ using microwave manipulation of the electronic spin.

To calculate the effect of the first interaction we apply the BCH formula to ρ_1^0 given by (3.57) with

$$\left[H_{\text{eff}}, \rho_1^0\right] = iS_y \otimes \tfrac{1}{2}I_x, \quad \Delta = S_e \otimes I_e.$$

Thus, we obtain

$$\rho_2^0 = S_y \sin\alpha \otimes I_x + (S_e + S_x \cos\alpha) \otimes I_e, \qquad (3.58)$$

and after the $\pi/2$ pulse along S_x we get

$$\rho_3^0 = S_z \sin\alpha \otimes I_x + (S_e + S_x \cos\alpha) \otimes I_e. \qquad (3.59)$$

Considering S_z as an observable with eigenvalues and projections given by (3.38), we can *predict*, using von Neumann's canonical rule (sometimes also called Bayesian estimation), the *a posteriori* state of the system:

$$\rho_+(0) = \frac{(S^\alpha \otimes \mathbb{1})\rho^1(S^\alpha \otimes \mathbb{1})}{\mathbb{P}_0^{S_z}(\lambda_+)} = (S_e + S_z) \otimes (I_e + \sin\alpha I_x),$$
$$(3.60)$$

$$\rho_-(0) = \frac{(S^\beta \otimes \mathbb{1})\rho^1(S^\beta \otimes \mathbb{1})}{\mathbb{P}_0^{S_z}(\lambda_-)} = (S_e - S_z) \otimes (I_e + \sin\alpha I_x).$$
$$(3.61)$$

The probabilities of occurrence of the eigenvalues λ_+ and λ_- are given by

$$\mathbb{P}_0^{S_z}(\lambda_+) = \text{tr}[S^\alpha \rho^1] = \tfrac{1}{2},$$
$$\mathbb{P}_0^{S_z}(\lambda_-) = \text{tr}[S^\beta \rho^1] = \tfrac{1}{2}. \qquad (3.62)$$

Since no projective readout is performed at this stage, our knowledge of the state of the system is limited to the information that, with a probability of $1/2$, the nuclear spin is in a state of incomplete polarization either in direction $|0\rangle$ or in direction $|1\rangle$. Nevertheless, this information is adequate to the calculating the correlation function of the output process in the POVM measurement scheme.

In what follows, we will use the notation [compare (3.16)]

$$\rho_\pm(0) = (S_e + S_z) \otimes (I_e \pm I_x \sin\alpha) \qquad (3.63)$$

for this state. Having done the calculations of Sec. III B with the replacement of $x = \cos(\omega t_f)$ by $x = \pm \sin\alpha \cos(\omega t_f)$, it is easy to obtain a modification of expression (3.48):

$$x_N^\pm \approx \pm \sin\alpha \cos(\omega N t_f) \exp\left[-\frac{(N-1)\alpha^2}{4}\right], \qquad (3.64)$$

which we use below when calculating the correlation function. In this case the output process is given by

$$\zeta_N = \text{tr}[\sigma_z \rho^S(N)] = x_N^\pm \sin\alpha$$
$$\approx \pm \sin^2\alpha \cos(\omega N t_f) \exp\left[-\frac{(N-1)\alpha^2}{4}\right]. \qquad (3.65)$$

E. Autocorrelation of observables I_x and S_z and relative entropy

The autocorrelation function of a classical random process is defined as the second moment of the joint distribution. In quantum mechanics, the definition of a joint distribution in the classical sense is meaningless due to the impossibility of (exact) simultaneous measurements of noncommuting observables in the framework of projective von Neumann measurements. Nevertheless, this problem is solved in terms of the positive operator value measures in the way, which is a natural consequence of conventional ideas of quantum theory (see [36] and Appendix C).

We intend to calculate the correlation of the output process $\{\zeta_n\}$ given by (3.65). However, since its probabilistic properties are completely determined by the sequence $\{x_N^\pm\}$ (3.64), we will deal with the calculation of correlations for

this process associated with the observable I_x. It means that, depending on the realized sign of the polarization, all measurements are determined either by the sequence $\{x_N^+\}$ or by the sequence $\{x_N^-\}$.

First of all, we note that the probabilities of realizing $\{x_N^+\}$ or $\{x_N^-\}$ are determined by the probabilities (3.62):

$$\mathbb{P}(x_N^-) = \mathbb{P}_0^{S_z}[\lambda_+] = \tfrac{1}{2},$$
$$\mathbb{P}(x_N^-) = \mathbb{P}_0^{S_z}[\lambda_-] = \tfrac{1}{2}. \qquad (3.66)$$

Recall that observable I_x has eigenvalues $\mu_+ = \tfrac{1}{2}$, $\mu_- = -\tfrac{1}{2}$ with the eigenvectors

$$|0\rangle = \frac{1}{\sqrt{2}}(1,0)^T, \quad |1\rangle = \frac{1}{\sqrt{2}}(0,1)^T \qquad (3.67)$$

and corresponding projection operators $I_x^\alpha := I_e + I_x$, $I_x^\beta := I_e - I_x$, given by

$$I_x^\alpha = \frac{1}{2}\begin{bmatrix} 1 & 1 \\ 1 & 1 \end{bmatrix}, \quad I_x^\beta = \frac{1}{2}\begin{bmatrix} 1 & -1 \\ -1 & 1 \end{bmatrix}. \qquad (3.68)$$

The measurements of the observable $I_x = \mu_+ I_x^\alpha + \mu_- I_x^\beta$ corresponding to the projectors I_x^α and I_x^β are given by the probabilities [compare (3.39)]

$$\mathbb{P}_N^{I_x}[\mu_+|x_N^\pm] = \mathbb{P}_N^{I_x}[\mu_+|\lambda_\pm] = \text{tr}[I_x^\alpha \rho_\pm^I(N)],$$
$$\mathbb{P}_N^{I_x}[\mu_-|x_N^\pm] = \mathbb{P}_N^{I_x}[\mu_-|\lambda_\pm] = \text{tr}[I_x^\beta \rho_\pm^I(N)], \qquad (3.69)$$

where $\rho_\pm^I(N) = I_e + x_N^\pm I_x + y_N^\pm I_y$ corresponds (with obvious modification) to the density matrix (3.40) obtained for the case of deterministic polarization.

Thus, by direct calculation we find that the probabilities $\mathbb{P}_N^{I_x}[\mu_\pm|\lambda_\pm]$ are given by

$$\mathbb{P}_N^{I_x}[\mu_+|\lambda_+] = \text{tr}[I_x^\alpha \rho_+^I(N)] = \tfrac{1}{2}(1+x_N),$$
$$\mathbb{P}_N^{I_x}[\mu_+|\lambda_-] = \text{tr}[I_x^\alpha \rho_-^I(N)] = \tfrac{1}{2}(1-x_N),$$
$$\mathbb{P}_N^{I_x}[\mu_-|\lambda_+] = \text{tr}[I_x^\beta \rho_+^I(N)] = \tfrac{1}{2}(1-x_N),$$
$$\mathbb{P}_N^{I_x}[\mu_-|\lambda_-] = \text{tr}[I_x^\beta \rho_-^I(N)] = \tfrac{1}{2}(1+x_N), \qquad (3.70)$$

where $x_N := \sin\alpha \cos(\omega N t_f) \exp\left[-\frac{(N-1)\alpha^2}{4}\right]$.

Using (3.70), we define the probabilities $p^{I_x}(\mu_\pm, \lambda_\pm)$ to obtain the value corresponding to the state $\rho^I(N)$ *together* with the value, corresponding to the state $\rho^I(0)$ by Bayes' rule

$$p^{I_x}(\mu_+, \lambda_+) = \mathbb{P}_N^{I_x}[\mu_+|\lambda_+] \, \mathbb{P}_0^{S_z}[\lambda_+]$$
$$= \tfrac{1}{2}(1+x_N) \, \mathbb{P}_0^{S_z}[\lambda_+],$$
$$p^{I_x}(\mu_+, \lambda_-) = \mathbb{P}_N^{I_x}[\mu_+|\lambda_-] \, \mathbb{P}_0^{S_z}[\lambda_-]$$
$$= \tfrac{1}{2}(1-x_N) \, \mathbb{P}_0^{S_z}[\lambda_-],$$
$$p^{I_x}(\mu_-, \lambda_+) = \mathbb{P}_N^{I_x}[\mu_-|\lambda_+] \, \mathbb{P}_0^{S_z}[\lambda_+]$$
$$= \tfrac{1}{2}(1-x_N) \, \mathbb{P}_0^{S_z}[\lambda_+],$$
$$p^{I_x}(\mu_-, \lambda_-) = \mathbb{P}_N^{I_x}[\mu_-|\lambda_-] \, \mathbb{P}_0^{S_z}[\lambda_-]$$
$$= \tfrac{1}{2}(1+x_N) \, \mathbb{P}_0^{S_z}[\lambda_-]. \qquad (3.71)$$

Substituting (3.66) into (3.71), we obtain a set of probabilities that determine the *joint distribution* $p^{I_x}(\mu_\pm, \mu_\pm)$:

$$p^{I_x}(\mu_+, \lambda_+) = \tfrac{1}{4}(1 + x_N), \quad p^{I_x}(\mu_+, \lambda_-) = \tfrac{1}{4}(1 - x_N),$$

$$p^{I_x}(\mu_-, \lambda_+) = \tfrac{1}{4}(1 - x_N), \quad p^{I_x}(\mu_-, \lambda_-) = \tfrac{1}{4}(1 + x_N).$$

$$(3.72)$$

We define the autocorrelation of the process corresponding to observable I_x as

$$C^{I_x}(0, N) = \sum_{\pm, \pm} \mu_\pm \lambda_\pm \, p^{I_x}(\mu_\pm, \lambda_\pm). \quad (3.73)$$

Substituting now expressions (3.72) in (3.73) we obtain

$$C^{I_x}(0, N) = x_N$$

$$= \sin \alpha \cos(\omega N t_f) \exp\left[-\frac{(N-1)\alpha^2}{4}\right]. \quad (3.74)$$

Considering the connection (3.65) of the registered process ζ_N and the process $x_N^\pm$, it is now easy to obtain an expression for the correlation function of the output signal

$$C^{S_z}(0, N) = x^N \sin \alpha$$

$$= \sin^2 \alpha \cos(\omega N t_f) \exp\left[-\frac{(N-1)\alpha^2}{4}\right]. \quad (3.75)$$

In Appendix C we introduce an analog of the classical *relative entropy* of Kullback and Leibler (C12) as a measure of the discrepancy of information that occurs during the measurement process. We will now apply this formula to our particular case.

The information that we intended to obtain during the measurement is the initial value $x = \cos \omega t_f$ of the amplitude of the observable I_x. During the measurement process, after N steps, this information was translated with inevitable distortions into the amplitude ζ_N of the observable S_z, determined by the expression (3.65), and then was registered as a result of optical readout. Without loss of generality, we restrict ourselves for simplicity to the case of a polarized initial condition. In this case, measurements of the observable S_z instead of four conditional probabilities in (3.70) generate only a pair of unconditional probabilities given by the formulas (recall that λ_+, λ_- correspond to the projections S^α, S^β of the observable S_z)

$$\mathbb{P}_N^{S_z}[\lambda_+] = \tfrac{1}{2}(1 + x_N \sin \alpha),$$

$$\mathbb{P}_N^{S_z}[\lambda_-] = \tfrac{1}{2}(1 - x_N \sin \alpha). \quad (3.76)$$

An "ideal" measurement of the observable I_x in the state $\rho^I(1) = I_e + I_x \cos(\omega t_f) + I_y \sin(\omega t_f)$ gives two probabilities:

$$\mathbb{P}^{I_x} = \tfrac{1}{2}[1 + \cos(\omega t_f)] \quad \text{and} \quad \mathbb{P}^{I_x} = \tfrac{1}{2}[1 - \cos(\omega t_f)].$$

Hence, we get the following expression for the relative entropy:

$$H(S_z | I_x) = \frac{1}{2}(1 + x_N \sin \alpha) \log \frac{1 + x_N \sin \alpha}{1 + \cos(\omega t_f)}$$

$$+ \frac{1}{2}(1 - x_N \sin \alpha) \log \frac{1 - x_N \sin \alpha}{1 - \cos(\omega t_f)}. \quad (3.77)$$

The Taylor expansion of the function $\log(1 + y)$ gives a very simple and intuitive interpretation of the relative entropy in

terms of the weighted differences

$$(x_N \sin \alpha)^k - [\cos(\omega t_f)]^k$$

of all powers of the functions $x_N \sin \alpha$ and $\cos(\omega t_f)$ characterizing the discrepancy between the true and measured values.

APPENDIX A: MATHEMATICAL FORMULATIONS OF THE WIGNER-BELL THEOREMS

We will give a proof of the theorem based on formula (1.1), which just characterizes the difference between the classical probability, for which it is valid, and the quantum (noncommutative) probability.

Theorem A.1 (The Wigner-d'Espagnat inequality). Let ξ, ϕ, θ be arbitrary random variables with values ± 1 on a Kolmogorov probability space $(\Omega, \mathcal{F}, \mathbb{P})$. Then the following inequality holds:

$$\mathbb{P}(\xi = +1, \phi = +1) + \mathbb{P}(\phi = -1, \theta = +1)$$

$$\geqslant \mathbb{P}(\xi = +1, \theta = +1). \quad (A1)$$

Proof. Consider the following sets:

$$A = \{\xi = 1, \phi = 1, \theta = 1, \theta = -1\}, \quad (A2)$$

$$B = \{\xi = 1, \xi = -1, \phi = -1 \theta = 1\}, \quad (A3)$$

$$A \cap B = \{\xi = 1, \theta = 1\}, \quad (A4)$$

$$A \cup B = \{\xi = 1, \xi = -1, \phi = 1, \phi = -1, \theta = 1, \theta = -1\}. \quad (A5)$$

Hence, by (I1) we have

$$\mathbb{P}(A) + \mathbb{P}(B) = \mathbb{P}(A \cap B) + \mathbb{P}(A \cup B).$$

But since the set A contains both values of θ and the set B contains both values of ξ, this equality is equivalent to the following representation:

$$\mathbb{P}\{\xi = 1, \phi = 1\} + \mathbb{P}\{\phi = -1, \theta = 1\}$$

$$= \mathbb{P}\{\xi = 1, \theta = 1\} + \mathbb{P}(A \cup B), \quad (A6)$$

and due to the nonnegativity of the probability, we get

$$\mathbb{P}\{\xi = 1, \phi = 1\} + \mathbb{P}\{\phi = -1, \theta = 1\}$$

$$\geqslant \mathbb{P}\{\xi = 1, \theta = 1\}. \quad (A7)$$

∎

APPENDIX B: MODIFICATION OF THE BAKER-CAMPBELL-HAUSDORFF FORMULA

We show that under conditions

$$B = [H, A], \quad [H, B] = kA - k\Delta, \tag{B1}$$

$$[H, \Delta] = 0 \quad [H, [H, B] + k\Delta] = [H, [H, B]], \tag{B2}$$

the following modification of the BCH formula holds:

$$UAU^* = e^{-iH\phi} A e^{iH\phi} = A \cos(\phi\sqrt{k}) + \Delta[1 - \cos(\phi\sqrt{k})] - \frac{1}{\sqrt{k}} iB \sin(\phi\sqrt{k}). \tag{B3}$$

By direct calculation

$$UAU^* = e^{-iH\phi} A e^{iH\phi} = A - (i\phi)[H, A] + \frac{(i\phi)^2}{2!}[H, [H, A]] + \frac{(i\phi)^3}{3!}[H, [H, [H, A]]] + \cdots$$

$$= \left(A + \frac{(i\phi)^2}{2!}[H, B] + \frac{(i\phi)^4}{4!}[H, [H, [H, B]]] + \cdots \right) - \left(i\phi[H, A] + \frac{(i\phi)^3}{3!}[H, [H, B]] + \cdots \right)$$

$$= \left(A + \frac{(i\phi)^2}{2!}(kA - k\Delta) + \frac{(i\phi)^4}{4!}[H, [H, k(A - k\Delta)]] + \cdots \right) - \left(i\phi[H, A] + \frac{(i\phi)^3}{3!}[H, (kA - k\Delta)] + \cdots \right).$$

Since $[H, \Delta] = 0$ we write

$$UAU^* = \left(A + \frac{(i\phi)^2}{2!}(kA - k\Delta) + \frac{(i\phi)^4}{4!}[H, [H, kA]] + \cdots \right) - \left(i\phi[H, A] + \frac{(i\phi)^3}{3!}[H, kA] + \cdots \right)$$

$$= \left(A + \frac{(i\phi)^2}{2!}(kA - k\Delta) + \frac{(i\phi)^4}{4!}k[H, B] + \cdots \right) - \left(i\phi B + \frac{(i\phi)^3}{3!}kB + \cdots \right).$$

Next we use $[H, B] = kA - k\Delta$ to get

$$\left(A + \frac{(i\phi)^2}{2!}(kA - k\Delta) + \frac{(i\phi)^4}{4!}k(kA - k\Delta) + \cdots \right) - B\left(i\phi + \frac{(i\phi)^3}{3!}k + \cdots \right)$$

$$= A\left(1 + \frac{(i\phi)^2}{2!}k + \frac{(i\phi)^4}{4!}k^2 + \cdots \right) + \Delta\left(-\frac{(i\phi)^2}{2!}k - \frac{(i\phi)^4}{4!}k^2 + \cdots \right) - B\left(i\phi + \frac{(i\phi)^3}{3!}k + \cdots \right)$$

$$= A\left(1 - \frac{\phi^2}{2!}k + \frac{\phi^4}{4!}k^2 + \cdots \right) - \Delta\left(1 - 1 - \frac{\phi^2}{2!}k + \frac{\phi^4}{4!}k^2 + \cdots \right) - B\left(i\phi - \frac{(i\phi)^3}{3!}k + \cdots \right)$$

$$= A\left(1 - \frac{\phi^2}{2!}k + \frac{\phi^4}{4!}k^2 + \cdots \right) + \Delta - \Delta\left(1 - \frac{\phi^2}{2!}k + \frac{\phi^4}{4!}k^2 + \cdots \right) - B\left(i\phi - \frac{(i\phi)^3}{3!}k + \cdots \right)$$

$$= A \cos(\phi\sqrt{k}) + \Delta[1 - \cos(\phi\sqrt{k})] - \frac{1}{\sqrt{k}} iB \sin(\phi\sqrt{k}).$$

APPENDIX C: POVM MEASUREMENTS

Let Ω be a set with a σ field $\mathcal{F}$, $\mathcal{H}$ be a Hilbert space and $\mathcal{B}_{sa}(\mathcal{H})$ be a space of bounded self-adjoint operators in $\mathcal{H}$. A positive operator valued (POV) measure on Ω is defined to be a map $F : \Omega \to \mathcal{B}_{sa}(\mathcal{H})$ such that for $\Delta \in \mathcal{F}$, $F(\Delta) \geqslant F(\varnothing)$, and if $\{\Delta_n\}$ is a countable family of disjoint sets in $\mathcal{F}$ then

$$F\left(\bigcup_n \Delta_n \right) = \sum_n F(\Delta_n),$$

where the series converges in the weak operator topology.

POV measures naturally arise in the process of repeated (weak) measurements of some quantum observables (see Sec. III B), the scheme of which is described below. This process is implemented on the composite Hilbert space $\mathcal{H} =$ $\mathcal{H}_D \otimes \mathcal{H}_Q$ by coupling the primary quantum system Q, initially in the ρ state, on the Hilbert space $\mathcal{H}_Q$, to a quantum measuring device D, initially in the state

$$\sigma = \sum_k \lambda_k |e_k\rangle\langle e_k|, \tag{C1}$$

where the states $|e_k\rangle$ form an orthonormal basis for the Hilbert space $\mathcal{H}_D$ of the meter. The two systems interact during a period τ under the control of some Hamiltonian, and the result of the interaction is described by the unitary operator U *acting on the composite system*. After interaction the initial density matrix is transformed into

$$\rho_{QD}(\tau) = U(\tau)\rho \otimes \sigma U^*(\tau). \tag{C2}$$

The final projection measurement is determined by orthogonal projectors $\{P_\alpha\}$

$$P_\alpha = \sum_j |\phi_j^\alpha\rangle\langle\phi_j^\alpha|, \quad \alpha \in \mathbb{Z},$$

associated with a *measurable observable* $\mathcal{A}$ of the meter. Here the states $|\phi_j^\alpha\rangle$ form an orthonormal basis for the Hilbert space $\mathcal{H}_D$ of the meter and satisfy the completeness relation

$$\sum_{\alpha,j} |\phi_j^\alpha\rangle\langle\phi_j^\alpha| = \sum_\alpha P_\alpha = \mathbb{1}_{H_D} \tag{C3}$$

(compare the observable S_z and projections $S^\alpha = S_e + S_z$, $S^\beta = S_e - S_z$ in Sec. III B). The postmeasurement state of the *primary system* is obtained by taking a partial trace with respect to D:

$$\mathrm{tr}_D(P_\alpha U \rho \otimes \sigma U^* P_\alpha) = \mathrm{tr}_D(P_\alpha U \rho \otimes \sigma U^*) = S_\alpha(\rho). \tag{C4}$$

The probability to obtain result α in the measurement *on the meter* is dictated by the standard von Neumann rules for the orthogonal projectors measurement:

$$\mathbb{P}_{\rho\otimes\sigma}(\alpha) = \mathrm{tr}[P_\alpha U \rho \otimes \sigma U^*] := \mathrm{tr}[S_\alpha(\rho)]. \tag{C5}$$

Thus, the basic characterization of the measurement model is given by the quantum operation S_α, which is the linear transformation of the initial state

$$\rho \to S_\alpha(\rho). \tag{C6}$$

Substituting (C1) and (C3) in (C4) we get

$$\begin{aligned} S_\alpha(\rho) &= \sum_{j,k} \lambda_k^{1/2}\langle\phi_j^\alpha|U|e_k\rangle\rho\langle e_k|U^*|\phi_j^\alpha\rangle\lambda_k^{1/2} \\ &= \sum_{j,k} M_{jk}^\alpha \rho (M_{jk}^\alpha)^*. \end{aligned} \tag{C7}$$

The set of operators $M_{jk}^\alpha = \sqrt{\lambda_k}\langle\phi_j^\alpha|U|e_k\rangle$ provides a *Kraus decomposition* of the operation S_α, which in turn defines the set of effects F_α given by

$$\begin{aligned} F_\alpha &:= \sum_{j,k} (M_{jk}^\alpha)^* M_{jk}^\alpha = \sum_{j,k} \lambda_k\langle e_k|U^*|\phi_j^\alpha\rangle\langle\phi_j^\alpha|U|e_k\rangle \\ &= \mathrm{tr}_D[U^* P_\alpha U \sigma]. \end{aligned} \tag{C8}$$

The Kraus operators and hence the set of effects $\{F_\alpha\}$ satisfy a completeness relation:

$$\begin{aligned} \sum_{\alpha,j,k} (M_{jk}^\alpha)^* M_{jk}^\alpha &= \sum_{\alpha,j,k} \lambda_k\langle e_k|U^*|\phi_j^\alpha\rangle\langle\phi_j^\alpha|U|e_k\rangle \\ &= \mathrm{tr}_D(U^*U\sigma) = \mathrm{tr}(\mathbb{1}\otimes\sigma) = \mathbb{1}. \end{aligned} \tag{C9}$$

The probability to obtain result α in the measurement on the ancilla can now be written as

$$\begin{aligned} \mathbb{P}_{\rho\otimes\sigma}(\alpha) &= \mathrm{tr}[S_\alpha(\rho)] = \mathrm{tr}\left[\rho\sum_{j,k}(M_{jk}^\alpha)^* M_{jk}^\alpha\right] \\ &= \mathrm{tr}[\rho \cdot \mathrm{tr}_D[U^* P_\alpha U \sigma]] = \mathrm{tr}[\rho F_\alpha]. \end{aligned} \tag{C10}$$

Therefore, *we may identify a set of effects $\{F_\alpha\}$ or, equivalently, a set of Kraus operators $\{M_{jk}^\alpha\}$ with a generalized observable*

in the sense that the operator

$$R(E) = \sum_{\alpha\in E} F_\alpha, \quad E \subset \mathbb{Z} \tag{C11}$$

is a *positive operator-valued measure* and

$$\mathbb{P}_{\rho\otimes\sigma}(E) = \mathrm{tr}[\rho R(E)], \quad E \subset \mathbb{Z}.$$

Equation (C10) demonstrates that quantum observables are defined and measured relative to a reference frame (ancillas) and therefore can be considered as relative attributes.

Thus, the quantity F_α of a physical system is actually identified by the real experimental equipment used to measure the system. The relative nature of the observable, associated with *effects* $\{F_\alpha\}$, suggests the introduction of relative entropy as a measure of information transforming from (immeasurable) observable, related to the prime system, and a measurable observable $\mathcal{A}$, set by projections P_α related to the detector.

Let us assume that the observable $\mathcal{O}$ associated with the prime system, which is not accessible for direct measurement, is given by the projectors $\{Q_\alpha\}$ and that the unitary transformation U in (C2) defining the measurement process uniquely connects the projectors Q_α and $\{P_\alpha\}$ by some relation (compare the observables I_x and S_z and their projectors in Sec. III B). By analogy with commutative probability theory we define the *relative entropy* (also called information divergence and introduced in classical probability by Kullback and Leibler [50]) by

$$\begin{aligned} H(\mathcal{A}|\mathcal{O}) &= \sum_\alpha \mathbb{P}_{\rho\otimes\sigma}(\alpha)\log\frac{\mathbb{P}_{\rho\otimes\sigma}(\alpha)}{\mathbb{P}_\rho(\alpha)} \\ &= \sum_\alpha \mathrm{tr}[\rho F_\alpha][\log\mathrm{tr}[\rho F_\alpha] - \log\mathrm{tr}[\rho Q_\alpha]]. \end{aligned} \tag{C12}$$

Recall that in the noncommutative case for an isolated system the relative entropy of a state ω with respect to another state φ is usually defined in terms of the corresponding density operators by ρ_ω and ρ_φ:

$$H(\omega|\varphi) = \mathrm{tr}[\rho_\omega[\log\rho_\omega - \log\rho_\varphi]].$$

APPENDIX D: THE WEYL-WIGNER TRANSFORMATION AND APPROXIMATE OBSERVABLES IN THE PHASE SPACE REPRESENTATION

Let $H = L^2(\mathbb{R})$, be the Hilbert space, $\psi \in L^2(\mathbb{R})$ a state of a quantum system, and $\alpha \in L^2(\mathbb{R})$ a function of norm one, whose expectation is zero. *This function can be regarded as specifying certain limitations of the measurement device.* If we define a function

$$\alpha_{xy} = e^{iyq}\alpha(q - x), \tag{D1}$$

where the factor $\exp(iyq)$ simply maps the measurement uncertainty given by α from the Hilbert space into the phase space, then for any density operator ρ the *nonnegative* continuous function $\rho_\alpha(x, y)$ on phase space given by ($\langle\cdot,\cdot\rangle_L^2$ is a scalar product in L^2)

$$\rho_\alpha(x, y) := \frac{1}{2}\langle\rho\alpha_{xy}, \alpha_{xy}\rangle_{L^2} \tag{D2}$$

is a probability density on $\mathbb{R}^2$

$$\int_{\mathbb{R}^2} \rho_\alpha(x, y) \, dx \, dy = 1.$$

Recall that the Weyl operator $W(u, v)$ is defined on $L^2(\mathbb{R})$ by

$$(W(u, v)\psi)(x) = (e^{iuQ+ivP}\psi)(x). \qquad \text{(D3)}$$

The following statement is due to Davis [36]:

Let $\rho_\alpha(x, y)$ be the probability density of the state ρ on phase space defined by (D2) Then

$$\int_{\mathbb{R}^2} \rho_\alpha(x, y)e^{ixu+iyv} \, dx \, dy = \text{tr}[\rho e^{iuQ+ivP}]\langle\alpha, W(u, v)\alpha\rangle_{L^2}. \qquad \text{(D4)}$$

The Wigner density φ^W of a state ρ is defined formally by the equation

$$\int_{\mathbb{R}^2} \varphi^W(x, y)e^{ixu+iyv} \, dx \, dy = \text{tr}[\rho e^{iuQ+ivP}]. \qquad \text{(D5)}$$

In other words, the Wigner density is the inverse Fourier transform of the characteristic function $\text{tr}[\rho e^{iuQ+ivP}]$. If we define a function $\sigma_\alpha(x, y)$ by

$$\int_{\mathbb{R}^2} \sigma_\alpha(x, y)e^{ixu-iyv} \, dx \, dy = \langle\alpha, W(u, v)\alpha\rangle_{L^2},$$

then, taking the Fourier transforms, we can express $\rho_\alpha(x, y)$ as

$$\rho_\alpha(x, y) = \int_{\mathbb{R}^2} \rho_W(x - \xi, y - \eta)\sigma_\alpha(\xi, \eta) \, d\xi \, d\eta. \qquad \text{(D6)}$$

This shows that the probability density $\rho_\alpha(x, y)$ is the result of averaging the improper Wigner density by the function σ_α, which depends on the vector $\alpha \in L^2$ and reflects the inaccuracy of the measurements.

Recall that the conventional *position observable* on the Hilbert space $\mathcal{H} = L_2(\mathbb{R})$ is the projection-valued measure $q(\cdot)$ on $\mathbb{R}$, defined by

$$[q(B)\psi](x) = \chi_B(x)\psi(x), \quad \psi(x) \in L_2(\mathbb{R}), \qquad \text{(D7)}$$

where χ_B is the characteristic function of a Borel set $B \in \mathscr{B}(\mathbb{R})$. *The momentum observable* is *projection-valued measure* $p(\cdot)$ on $\mathbb{R}$, defined by

$$[p(B)\psi](x) = -i\chi_B(x)\partial_x\psi(x). \qquad \text{(D8)}$$

To formalize the random influence on measurements, a *probability density function* (known or unknown) $f(x)$ on $\mathbb{R}$ is introduced, and the convolution

$$(f * g)(x) = \int_{-\infty}^{\infty} f(y)g(x - y) \, dy \qquad \text{(D9)}$$

is defined for a bounded measurable function g on $\mathbb{R}$. It can be shown ([36], Theorem 3.1) that weakly convergent integrals (here $\hat{f}$ is the Fourier transform of f and $g \equiv \chi_E$)

$$Q_f(E) = \int_{\mathbb{R}} (f * \chi_E)(x)q(dx), \qquad \text{(D10)}$$

$$P_f(F) = \int_{\mathbb{R}} (\hat{f} * \chi_F)(k)p(dk) \qquad \text{(D11)}$$

uniquely define the so-called *approximate position and momentum observables* Q_f and P_f, which are POV measures on Borel sets E, F on $\mathbb{R}$. POV measures have the same properties as projection-valued (spectral) measures but *take values in the set of positive operators*, as the name suggests. It is clear that the approximate observables defined by (D10) and (D11) are commutative unsharp observables.

APPENDIX E: INFLUENCE OF STATE OF CHARGE

First, we explain qualitatively the effect of the charge state switching on the developed theoretical model. We assume that each green laser pulse can fully switch the charge state, meaning that the ionization rate at the power of 600 μW is around 3–5 MHz ($\approx 300^{-1}$ ns^{-1}), which results in switching times comparable to the duration of the laser pulse. We assume that there is a probability $p^- \approx 70\%$ of having NV$^-$ after the green pulse, independent of the history. Second, we assume that the charge state is stable during the "dark time" of the measurement when the laser is switched off. Next, we consider that the long-pass 650 nm filter in the detection pass cuts most of the NV^0 fluorescence spectra, making it darker compared to negative charge state. In the derivation of the correlation function, we use the fact that each measurement performs a measurement and hence imposes the back-action and causes the decay per measurement $\alpha^2/4$. The amplitude of the detected signal is given by the strength of the measurement $\sin\alpha$

The consequence of the charge state switching is thus twofold: (1) the missed $1 - p^-$ part of the measurement due to the NV^0 state will not perturb the target spin state, making the decay of the correlation function smaller $\alpha^2 p^-/4$, and (2) the amplitude of the correlation function $\langle S_z S_z \rangle$ will tend to be smaller by $(p^-)^2$, due to the reduction of "useful" data, produced by NV$^-$, and that S_z produces 0 when NV^0.

The latter effect is accounted by a contrast calibration procedure. The contrast shrinking of $\Delta n = p^-(n_a - n_b)$ will be observed as well, and when photon correlation $\langle n_i n_{i+k} \rangle$ is divided by the contrast Δn the full amplitude of the S_z correlation function will be restored under the assumptions that the p^- stays the same under both experiments, which is guaranteed by use of same NV and same laser pulses.

The former is more delicate as it affects the decay constant of the nuclear spin precession under the measurements by factor of p^-, which clearly becomes visible on longer correlation times. Thus, the process of fitting the correlation function S_z to the model function could give underestimated values of α, which could lead to systematic error in its estimated values.

To show this issue quantitatively, we simulate the process of sequential weak measurements with initially polarized target spin using the Monte Carlo method. We compare results for the model with the ideal case $p^- = 1.0(100\% \text{ NV}^-)$ and realistic case of $p^- = 0.7(70\% \text{ NV}^-)$ (see Fig. 5).

Using 1000 experimental runs of 100 weak measurements with $\alpha = 0.1\pi$ corresponding roughly to the KDD-XY3 sequence of NV^2, we estimate the average $\langle I_x \rangle(N)$ evolution in both cases. We observe that in the realistic case the decay is smaller; however, due to noise its significance becomes clear only at long correlation times.

Next, we fit the numerically obtained S_z data with a model function $\sin\alpha \cos(\omega t_s N)\exp(-\alpha^2 N/4)$ and find α_{est}. We di-
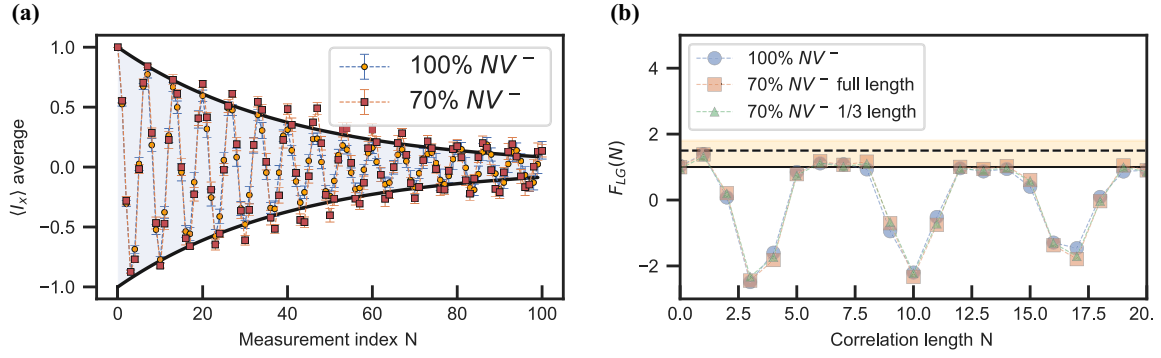
FIG. 5. The influence of the charge state dynamics on the I_x evolution. (a) The evolution of the I_x has smaller decay, which is shown by the red dots. Panel (b) shows a recovered L-G function using both data sets, including the value of α_{est} from the full data set and from the shortened I_x to $N = 30$. The cut plays important role, due to the less importance of the actual decay values.

vide the S_z by $\sin \alpha_{est}$ and get I_x reconstructed, and check the LG expression from them: $LG(N) = 2I_x(N) - I_x(2N)$.

Analyzing the reconstructed values we conclude that the errors induced by charge state are less than statistical errors and do not affect significantly the correlation function relevant for the first two periods of oscillation, the region which is essential for its violation of the inequality.

Additionally, we note that it is possible to optimize the fitting procedure by weighting the correlation function points depending on their correlation length; in particular, we find that use of the box car weighting (cutting the tail of the exponent) with window length equal to $1/3$ of the original decay gives a much better estimate of the alpha values, due to the fact that on this data set, initial amplitude is more important than the decay. We point out that this could be a subject of future research in the field.

APPENDIX F: CLASSICAL FIELD CALIBRATION

To calibrate the classical field amplitude, we perform AC sensing of a 2 MHz AC external field at various output power of the external generator from -18 to 2 dBm. We apply the KDD-XY5 sensing sequence. The algorithm is as following:

(1) $\rho_e = S_e + S_x$ state is prepared with a $\pi/2$ pulse which rotates the initially polarized $S_e + S_z$ state towards the equator.

(2) The phase acquired during the KDD sequence is estimated as

$$\Phi = \cos(\omega t + \phi)\text{sinc}(N_p \tau \pi \delta). \tag{F1}$$

(3) The $\pi/2$ pulse rotates the state around the y axis (again) and converts the X component of the state to the readable Z component. Hence

$$S_z = \cos \Phi = \cos[\alpha \cos(\omega t + \phi) \, \text{sinc}(N_p \tau \pi \delta)]. \tag{F2}$$

(4) We perform a series of measurements without controlling the phase and time; hence we average over the argument of $\cos(\omega t + \phi)$ which we denote as ϕ_s to derive the averaged result $S_z = \int_{\phi_s} \cos[\alpha \cos(\phi_s) \, \text{sinc}(N_p \tau \pi \delta)] d\phi_s = J_0[\alpha \, \text{sinc}(\delta N_p \pi \tau)]$.

(5) The readout of the state S_z is not ideal. It has losses of contrast due to the finite T_1 of the nuclear spin under the readout, and instability of the charge state reduces the full possible

contrast by constant K. Hence, we obtain an expression

$$S(\tau) = S_1 - S_2 = K J_0[\alpha \, \text{sinc}(N_p \tau \pi \delta)] \tag{F3}$$

which we fit to the absorption spectra of the external signal [see Fig. 6(a)].

Here α is the normalized field strength B_{rf}, ϕ is the phase of the signal at the beginning of the sequence, and τ is dynamical decoupling pulse spacing, i.e., the half period $0.5 f^{-1}$ of the artificial signal. The S_z component readout is performed via the memory-enhanced single-shot readout scheme (see Appendix H). After fitting the absorption profiles, we get a calibration of signal strength for various input powers on the signal generator for our setting [see Fig. 6(b)], fitted with expression $\alpha = \alpha_0 \exp(P_{dBm}/k)$. We compare the absorption method with a correlation measurement with the phase modulation scheme presented in the main text and find an agreement between them. For the -17 dBm signal power which was used for the experiment we got $\alpha_{abs} = 0.94(5)$ and $\alpha_{corr} = 0.88(4)$ rad respectively.

APPENDIX G: CASE OF POLARIZATION OF NUCLEAR SPIN

To experimentally study the case of a hyperpolarized initial state of a nuclear spin we first polarize the ^{13}C nuclear
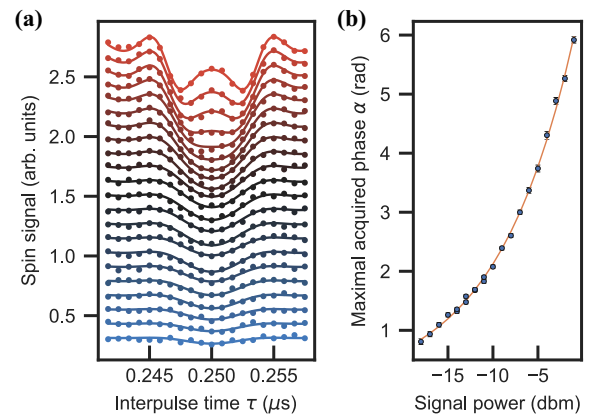

FIG. 6. External field amplitude calibration. (a) Absorption profiles of the KDD-XY5 sequence as a function of interpulse spacing τ for various signal amplitudes. (b) The extracted parameter α of the classical signal as a function of signal power on the r.f. generator.
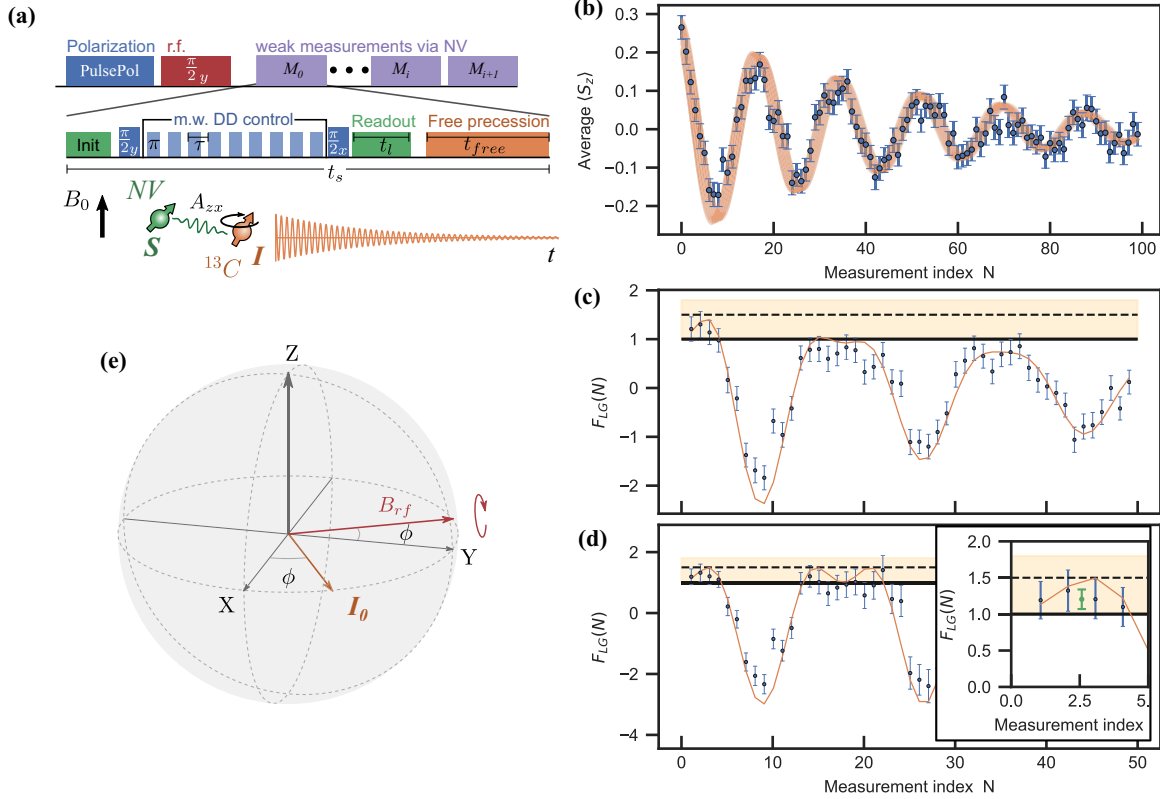
FIG. 7. (a) Sequential weak measurements of target spins with the prior polarization scheme. The sequence contains the Pulse-Pol routine as polarization, radio frequency (r.f.) $\pi/2$ pulse for initiating free precession of ^{13}C target spin, and sequence of weak measurements including the KDD-XY3 sequence for NV2 and ^{14}N polarization. (b) Average electron spin S_z in the series of measurements $M_0, \ldots, M_{N-1}, M_N$. Orange uncertainty area is a confidence interval of the fitting model. The uncertainty of the initial phase adds additional systematic parameter for calibration in this case, which is not present in the nonpolarized case. (c) The L-G expression of recovered I_x component of the nuclear spin. Note that in this case we took $\langle I_x \rangle$ as a K function of the L-G functional. (d) The L-G functional from the I_x signal divided by the exponential decay with $\exp(-\alpha^2 N/4)$. The error bars are also divided by exponential decay and express how well our model of an effective Hamiltonian describes the obtained signal. This view shows that the signal behaves according to the model for several intervals where inequality is violated. The inset shows the integral points of L-G inequality violation corresponding to the violation points on the main chart (first four points), which gives stronger confidence in violation. (e) Depiction of the initial phase with respect to the rotation frame of the nuclear spin drive on the Bloch sphere.

spin with a standard Pulse-Pol sequence [51] and saturate the polarization transfer from the electron spin by repeating the procedure four or five times after realigning the electron spin with laser light. Starting from the polarized nuclear state, we perform a $\pi/2$ rotation of the nuclear spin via radio frequency (r.f.). However, when driving the nuclear spin, the rotation instead of the x axis occurs around the direction $\mathbf{B_{rf}} = (-\sin\phi, \cos\phi, 0)$. Consequently, the polarized $I_e + I_z$ state transforms into the $I_e + \cos\phi I_x + \sin\phi I_y$ state, followed by precession in the equatorial plane of the Bloch sphere, as shown in Fig. 7(e). Therefore, the azimuthal angle ϕ corresponds to the initial phase of nuclear precession and must be taken into account in data analysis.

Note that in the case of a polarized initial state, since the initial condition is determined, the calculation of the correlation function reduces to the calculation of the average process $\langle S_z \rangle$. Therefore, during the nuclear spin precession we apply sequential weak measurements of nuclear spin $H_{\text{eff}} = 2\alpha S_z I_x$, and similarly to [25] calculate the averaged number of photons in a series of experiment. We estimate the $\langle S_z \rangle$ of the sensor electron spin, using the n_a and n_b values for electron spin

bright and dark state, measured separately. Note, however, that the formula for the unpolarized case was obtained under the assumption that the initial state is aligned with the x axis and therefore does not take into account the presence of the azimuth angle ϕ. In this regard, when processing the data, we used a modified model

$$S_z(N) \approx \sin\alpha \cos(\omega N t_f + \phi) \exp\left(-\frac{N}{4}\alpha^2\right). \quad \text{(G1)}$$

Then, following the same idea in the case of an unpolarized initial state, we reconstruct the mean value $\langle I_x \rangle$ and LG function shown in Fig. 7(c). Note again that in this case to obtain $\langle I_x \rangle$ we divide $\langle S_x \rangle$ by $\sin\alpha$ instead of $\sin^2\alpha$. We obtain an explicit violation of the LG inequality at three points in the first period; however, it should be taken into account that in this case there is an additional uncertainty associated with the presence of an unknown azimuth angle ϕ.

Since the formula of the correlation function explicitly contains the dephasing factor, the rate of which, given by α, is estimated in the experiment, it is natural to correct the correlation function by dividing by the exponential decay. If
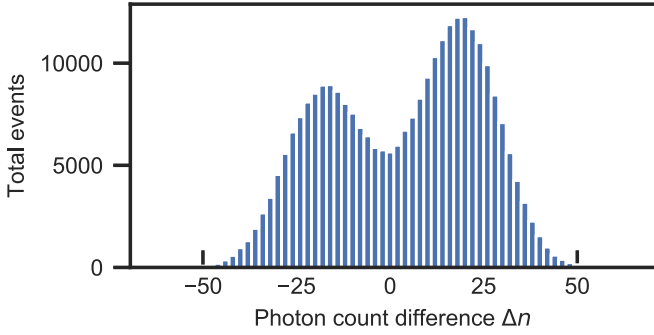
FIG. 8. Histogram of the photon count differences Δn in single-shot readout with referenced probing using two microwave π pulses, conditioned to $m_i = 0$ and $m_i! = 0$. In such a case the threshold is positioned on the $\Delta n = 0$.

the estimate of α is sufficiently accurate over some time interval, then the violation of the inequality should manifest itself over the entire this interval. Figure 7(d) shows one of these reconstructions. This figure shows that the signal behaves according to the model for several intervals where inequality is violated. A similar picture is observed in other experiments.

APPENDIX H: SSR METHOD FOR ESTIMATING THE α PARAMETER

The single-shot readout (SSR) method [45] can be considered as an analog of the maximum likelihood method in statistics and is used to reproduce an *ideal projective measurement*, in which individual measurements generate a sequence of 0 and 1, depending on the state of spin.

The NV center has ^{14}N as a built-in memory, where the state of the electron spin ρ_S can be mapped. The *transfer* of the electron spin state onto the nuclear spin is realized by a radio-frequency π pulse on the nuclear spin conditional on electron spin (CNOT gate). The SSR of the nuclear spin is carried out by repeating CNOT gates on the electron spin followed by a laser pulse readout. More precisely, we apply the microwave π pulse, which rotates the electron spin conditional on nuclear spin $|-1\rangle$, and then perform the green laser readout that projects the electron spin state and gives the number n_k^1 of photons associated with the projected state. The next microwave π pulse rotates the electron spin, conditional this time on $|0\rangle$ and $|+1\rangle$, and is then accompanied by a green readout, which gives the number of photons n_k^2 associated with the projected state. Finally, we calculate $\Delta_k = n_k^1 - n_k^2$. Whereas the electron spin state is destroyed each time during this process, the nuclear spin state is robust to repeat the measurements many times (we repeat the described process 900 times). This procedure of nondemolishing measurements permits one to gather enough statistics to estimate the nuclear spin state with the help the photon-counting histograms (see Fig. 8). When the readout assisted by the ^{14}N nuclear spin is applied and the interpulse time τ *is closed to the resonant* τ_0, then the number of photons in each cycle becomes quite large, and two peaks in the histogram become clearly distinguishable. This makes it possible to choose a threshold between spin states that corresponds to different peaks in the histogram (see Fig. 8).

As a result the output is recorded as $+1$ or -1 if the photon counts in a cycle are above or below a threshold

$$s_k^\pm = \begin{cases} +1 & \text{if } \Delta n_{k-1} \leqslant n_{th} \quad \text{and} \quad \Delta n_k > n_{th} \\ -1 & \text{if } \Delta n_{k-1} < n_{th} \quad \text{and} \quad \Delta n_k < n_{th}. \end{cases} \quad \text{(H1)}$$

The advantage of this method is that as a result we can calculate the normalized frequency

$$\hat{P}_{\alpha(\beta)} = \frac{\sum_k s_k^+}{\sum_k (s_k^+ + s_k^-)} \quad \text{(H2)}$$

of the flips. The normalized frequencies $\hat{P}_\alpha$ and $\hat{P}_\beta$ can be considered as an estimate of the probability of realization of the one of projections S^α or S^β in the *ideal projective measurement*, depending on what state was prepared in the sensing part of the experiment.

The *sensing part*, which is carried out on the electron spin using microwave pulses, is divided into two cases. Both cases start with the initial state of NV spin $\rho_S = S_0 + S_z$, which is then rotated to $\rho_S = S_0 + S_x$ by $(\pi/2)_y$ pulses around the y axis. The DD sequence with the different interpulse time τ is then applied to $\rho_S = S_0 + S_x$, and as a result the phase

$$\Phi = \alpha \cos(\omega t + \phi)\text{sinc}(N_p \tau \pi \delta) \quad \text{(H3)}$$

is acquired, where $\delta = \tau - \tau_0$ is a deviation of applied τ from a resonance time τ_0. The difference is that in one case the $(\pi/2)_y$ pulse around the y axis converts the amplitude of the x component of the state to the amplitude $+S_z$ of the readable z component, while in the second case the $(\pi/2)_{-y}$ pulse converts the amplitude of the x component of the state to the opposite $-S_z$ direction.

We perform the series of measurements of $\hat{P}_\alpha - \hat{P}_\beta$ for various τ and for the power external signal P_{dBm} varied from -18 to -2 dBm to determine the resonant frequency τ_0. It should be noted that the shape of the resonance curves for a weak and strong signal differs significantly.

Having revealed the near-resonant τ, we can proceed to determine the parameter α. The idea of estimating α is based on a comparison of the average value of the ideal projective measurement, which can be calculated using the SSR estimations of the probabilities $\hat{P}_\alpha$ and $\hat{P}_\beta$

$$\langle S_z \rangle_{\text{ideal}} = (+1)\hat{P}_\alpha + (-1)\hat{P}_\beta = \hat{P}_\alpha - \hat{P}_\beta, \quad \text{(H4)}$$

and the mean value of output macroscopic signal averaged over a random phase $E^\phi \langle S_z \rangle$ [see (H3)], which represents the conventional optical readout of S_z

$$E^\phi \langle S_z \rangle = \frac{1}{2\pi} \int_0^{2\pi} \cos[\alpha \cos(\omega t + \phi)\text{sinc}(\tau N_p \pi \delta)] \, d\phi$$
$$= J_0[\alpha \text{sinc}(\tau N_p \pi \delta)], \quad \text{(H5)}$$

where $J_0(x) = \frac{1}{\pi} \int_0^\pi \cos(x \sin t) \, dt$ is the Bessel function. Using the well-known dependence of the magnetic field B_z on the signal power P_{dBm}, we express α in terms of power $\alpha = 2B_z N_p \tau / \pi = \alpha_0 10^{P_{dBm}/P_0}$, where P_0 is a known normalizing parameter, while α_0 must be determined. We introduce the parameter K and perform a series of experiments at various values of P_{dBm}, selecting K and α_0 so that they satisfy

$$\min_{K, \alpha_0} |(\hat{P}_\alpha - \hat{P}_\beta) - K J_0[\alpha_0 10^{P_{dBm}/P_0}\text{sinc}(\tau N_p \pi \delta)]|^2. \quad \text{(H6)}$$
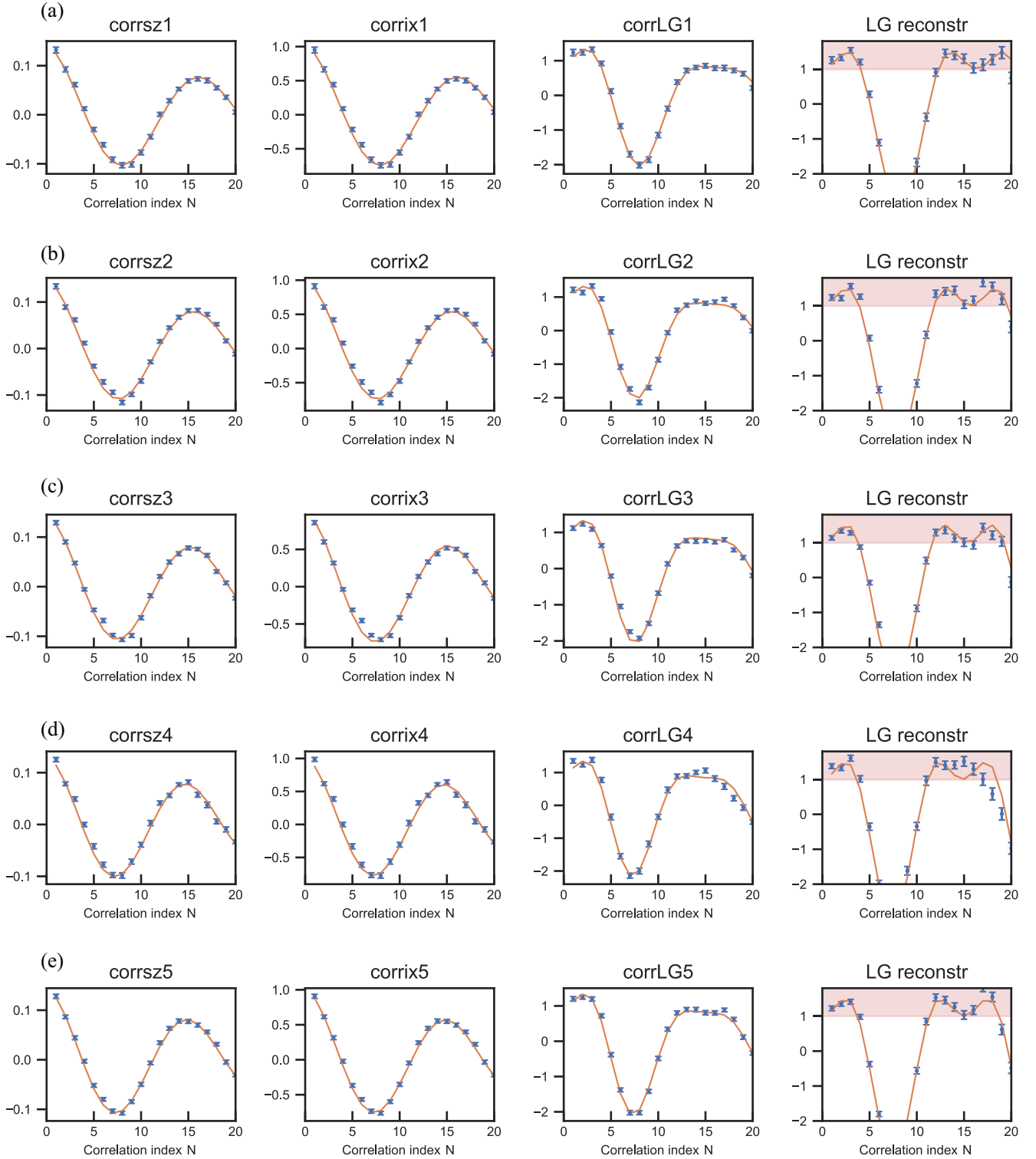
FIG. 9. Result of five series of main experiments on NV2 with KDD-XY5 and $N_{RR} = 200$ repetitive readouts using ^{14}N as an ancillary memory.

The parameter K can be considered as a parameter characterizing the transition from the quantum state to the classical probabilistic output in our particular experiment, which is determined by an inaccuracy in estimating the SSR probabilities $\hat{P}_{\text{alpha}}$, $\hat{P}_{\text{beta}}$ and possibly also by other factors that make real measurements invasive. It turns out that in our experiments the constant K is independent of power P_{dBm}, while the equality in (H6) is achieved with high accuracy. The dependence of alpha on the power calculated by this scheme is shown in [Fig. 6(b)].

As explained in the Appendix I: Data Analysis, to reconstruct the correlation function from a photon statistic by formula (I9) we need to determine the values $\langle n_+ \rangle$ and $\langle n_+ \rangle$ of
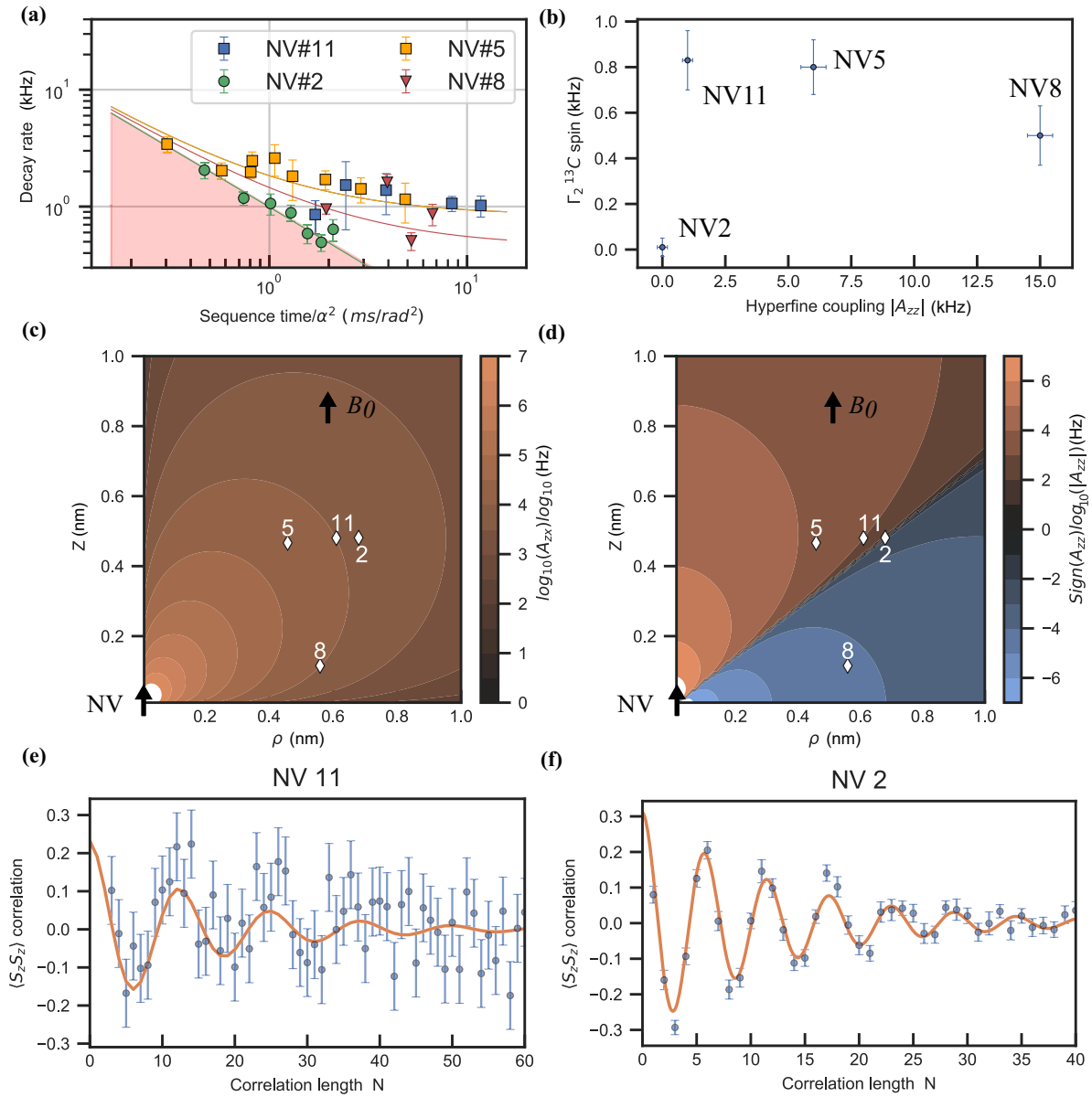
FIG. 10. Choice of NV-^{13}C pair. (a) Decay rate of the ^{13}C correlation signal in a sequence presented in Fig. 7(a) vs total sequence time t_s normalized by α^2 (measurement strength). Various ^{13}C possess a plateau, which was fitted and extracted as a natural Γ_2 rate for each ^{13}C at corresponding NV. (b). Dependence of the ^{13}C decay rate as a function of the A_{zz} coupling of the corresponding ^{13}C. (c), (d) Map of ^{13}C relative positions to their NV center. Note NV2 is located close to the magic-angle latitude with close to zero A_{zz}. (e), (f) The S_z correlation results for two NV11 and NV2, respectively. The signals show a clear difference in signal-to-noise ratio. The reason for that is overall better spin readout contrast of fluorescence for NV2, since the ^{14}N is polarized as well as reduced decay of the correlation signal due to vanishing A_{zz} coupling. Nonpolarized ^{14}N also leads to a shift in the readout phase of the KDD sequence, which ultimately reduces the contrast and even could change the underlying dynamics of the target spin.
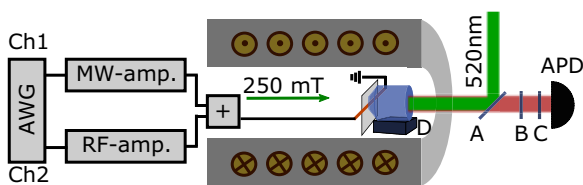
FIG. 11. Experimental setup scheme. A stands for a wedged mirror, B is a pinhole, C is a long pass filter 650 nm, D is the 3D piezo nanopositioner.

photon numbers. The numbers $\langle n_+ \rangle$ and $\langle n_+ \rangle$ are the specific readout characteristics of the NV center, which are independent of the magnetic field in the classical signal experiment or in the case of hyperfine interaction. Therefore, their measured values can be used in both experiments. To determine $\langle n_+ \rangle$ and $\langle n_+ \rangle$ we perform a series of measurements analogous to sequential measurements nonresonant to nuclear spin with additional modulation of the readout $\pi/2$ pulse phase. This periodically brings electron spin to states 1 and 0. After averaging we get the average photon numbers for bright and dark states.

We perform a series of measurements with the following protocol. First, we polarize the ^{14}N nuclear spin to the $|-1\rangle$ state by swapping electron spin polarization using selective π pulses and polarize the electron spin back with green laser light. We then apply $(\pi/2)_y$ pulse to the electron spin and the same DD sequence as in the correlation measurements. Finally, we apply $\pi/2_{x+\phi_m(i)}$, followed by optical green readout to collect photons.

The angle or phase ϕ determines the rotation axis in the x-y plane with respect to the y axis. In our measurement we set $\phi_m(k) = \pi/2 \sin(k2\pi/8)$, where k is the index of the measurement. Thus, the phase is modulated with amplitude of 90° and a period of eight measurements. We group these measurements in a series diagram in increments of 32 and then average columnwise to obtain the average photon number $\hat{n}_k$. As a result, the amplitude S_z of the density matrix ρ_S takes the form

$$S_z^k(\alpha, \Phi_s) = \sin[\pi/2 \sin(k2\pi/8) + \alpha \cos(\omega t + \phi_0)]$$
$$:= \sin[\pi/2 \sin(k2\pi/8) + \alpha \cos(k\Phi_s\pi/4)].$$

Note that S_z depends on the parameters α, Φ_s which we want to find. We use this result as a theoretical model of the measured signal, whose correlation function can be calculated at least numerically and calculate α, Φ_s, using the least-squares method

$$\min_{C,\alpha,\Phi_s} \sum_{k=1}^{200} \left(\langle (n_j - \hat{n})(n_{j+k} - \hat{n}) \rangle_j \right.$$
$$\left. - C^2 \langle S_z^j(\alpha, \Phi_s) S_z^{j+k}(\alpha, \Phi_s) \rangle_j \right)^2,$$

where $\{n_j\}$ are measured photon numbers, and $\hat{n}$ is average of measured photon number and $C = (n_a - n_b)/2$. Note that with this approach, we simultaneously calculate α and contrast $C = (n_a - n_b)/2$.

APPENDIX I: DATA ANALYSIS

The result of measurements in our experiment is a sequence $\{n_k\}$ of the number of photons recorded during each read-out. Thus, we need to find how the probabilistic properties of counting statistics $\{n_k\}$ are related to the probabilistic characteristics of the sensor signal $\{m_k\}$. Let $p(n_k|m_k)$ be the conditional probability of detecting n_k photons given that the electron spin is in the state that *would produce the output m_k under a perfect projective measurement*. The joint probability $p(n_k, n_{k+N})$ of the two outcomes n_k and n_{k+N} can be expressed through joint distribution $p(m_k, m_{k+N})$ as follows:

$$p(n_k, n_{k+N}) = \sum_{m_k, m_{k+N}} p(n_k|m_k)p(n_{k+N}|m_{k+N})p(m_k, m_{k+N}).$$

$$\text{(I1)}$$

Thus, the autocorrelation function of the process $\{n_k\}$ is given by

$$cor(n_k, n_{k+N}) := \langle n_k, n_{k+n} \rangle - \langle n_k \rangle \langle n_{k+N} \rangle, \quad \text{(I2)}$$

where, in view of (I1),

$$\langle n_k n_{k+N} \rangle := \sum_{n_k, n_{k+N}} n_k n_{k+N} p(n_k, n_{k+N})$$
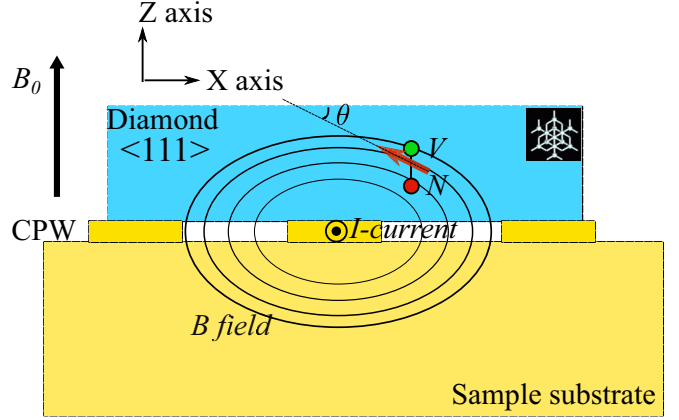

FIG. 12. Scheme of the diamond sample and NV center.

$$= \sum_{n_k, n_{k+N}} \sum_{m_k, m_{k+N}} n_k p(n_k|m_k) n_{k+N} p(n_{k+N}|m_{k+N})$$
$$\times p(m_k, m_{k+N}). \quad \text{(I3)}$$

Considering now the sequence $\{m_k\}$ as a classical stochastic output process as if we could measure it directly, we apply the *bivariate Bernoulli distribution model* to calculate $p(m_k, m_{k+N})$. For any m_k and m_{k+N}, the two-point joint distribution $p(m_k, m_{k+N})$ of elements of random process $\{m_k\}$ in this case is defined by the matrix

$$p(m_k, m_{k+N}) = \begin{bmatrix} P(-1, -1) & P(1, -1) \\ P(-1, 1) & P(1, -1) \end{bmatrix} = \begin{bmatrix} p_{00} & p_{10} \\ p_{01} & p_{11} \end{bmatrix}$$

with

$$p_{00} + p_{10} + p_{01} + p_{11} = 1. \quad \text{(I4)}$$

The marginal distribution of m_k is given by univariate law with parameter $p_{10} + p_{11}$,

$$P(m_k = -1) = p_{00} + p_{01} \quad P(m_k = +1) = p_{10} + p_{11},$$

and similarly the marginal distribution of m_{k+N} is

$$P(m_{k+N} = -1) = p_{00} + p_{10} \quad P(m_{k+N} = +1) = p_{01} + p_{11}.$$

We assume that $p_{00} = p_{11}$ and $p_{01} = p_{10}$. Then the mean value of m_k and m_{k+1} is

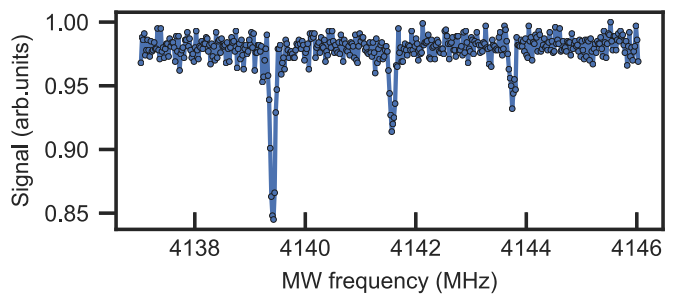$$E(m_k) = -1(p_{00} + p_{01}) + 1(p_{10} + p_{11}) = 0,$$

FIG. 13. Pulsed-ODMR spectra of the single NV center for $m_s = 0$ to $m_s = -1$ electron spin transition. ^{14}N nuclear spin hyperfine splitting of 2.2 MHz is visible. No visible hyperfine coupling for ^{13}C within T_2^*; π pulse is 8 μs.
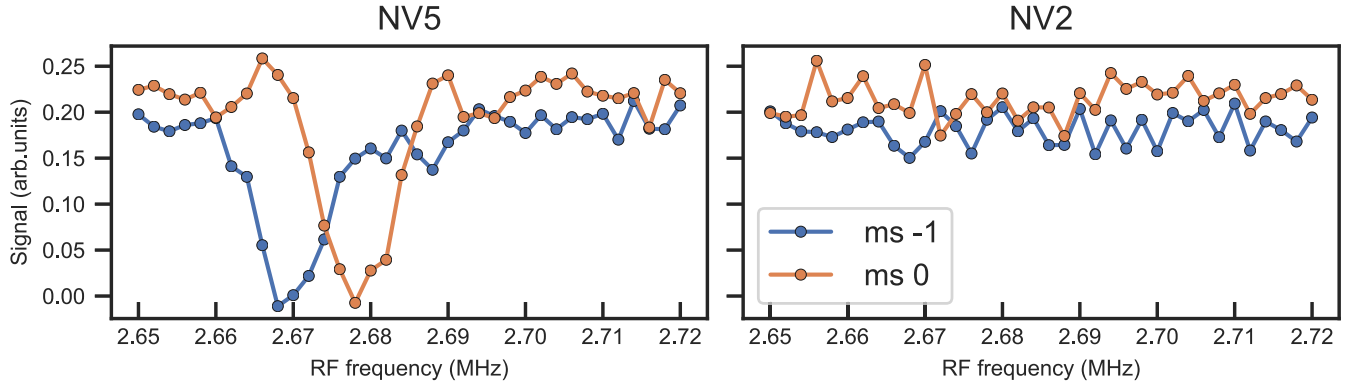
FIG. 14. ENDOR spectroscopy of two NV centers. NV5 is an example with detectable nuclear spin coupling for total interrogation time of 100 μs. NV2 is the NV center used in the current research without detectable A_{zz} coupled nuclear spin within the 100 μs total interrogation time.

and similarly $E(m_{k+N}) = 0$ for all k and N. Hence, the correlation function of the pair (m_k, m_{k+N}) is given by

$$E(m_k m_{k+N}) = (-1)(-1)p_{00} + 1(-1)p_{10}$$
$$+ (-1)(1)p_{01} + (1)(1 p_{11})$$
$$= (p_{00} + p_{11}) - (p_{10} + p_{01}), \qquad (I5)$$

or in compact form

$$E(m_k m_{k+N}) = [1 \quad -1] \begin{bmatrix} p_{00} & p_{10} \\ p_{01} & p_{11} \end{bmatrix} \begin{bmatrix} 1 \\ -1 \end{bmatrix}. \qquad (I6)$$

Since we consider $\{m_k\}$ as an output macroprocess, its autocorrelation function is given by

$$E(m_k m_{k+N}) := \sum_{m_k, m_{k+N}} m_k m_{k+N} p(m_k, m_{k+N}).$$

Thus, we can express the joint distribution $p(m_k, m_{k+N})$ through the autocorrelation $C(N)$ as follows:

$$p(m_k, m_{k+N})$$
$$= \begin{bmatrix} p_{00} = \frac{1}{4}[1 + C(N)] & p_{10} = \frac{1}{4}[1 - C(N)] \\ p_{01} = \frac{1}{4}[1 - C(N)] & p_{11} = \frac{1}{4}[1 + C(N)] \end{bmatrix}. \qquad (I7)$$

We do not need to know the exact form of $p(n_k|m_k)$, since we are interested only in a value of the average photon counts $\langle n_\pm \rangle$ for the NV center in the states $m_s = \pm$ given by

$$\langle n_\pm \rangle = \sum_{n_k} n_k p(n_k|\pm). \qquad (I8)$$

Thus, we conclude that in terms of the photon counting statistic $C(N)$ is given by (see [24])

$$C(N) = \frac{4(\langle n_k n_{k+N} \rangle - \langle n \rangle^2)}{(\langle n \rangle_+ - \langle n \rangle_-)^2}, \quad \langle n \rangle = (\langle n \rangle_+ + \langle n \rangle_-)/2.$$
$$(I9)$$

These considerations show that (under the assumptions made about the nature of the processes) probabilistic characteristics of processes $\{n_k\}$ and $\{m_k\}$ exhibit similar behavior. Therefore, information about the process $\{m_k\}$ can be extracted from photon statistics $\{n_k\}$, provided that we can measure the average values $\langle n \rangle_+$ and $\langle n \rangle_-$ with sufficient accuracy.

We collect a series of around 500 measurements, each of those is a coherent series of 200 000 sequential weak measurements. The size of 200 000 of each coherent series is motivated by hardware limitations.

The data processing is described in the Supplemental Material [52] (see Fig. 9).

APPENDIX J: NV-13C PAIR SURVEY

In addition to the ideal pair, designated NV2, the results of experiments which are given above, we also probed some other promising pairs, in particular, those marked as NV5, NV8, and NV11. Figures 10(c) and 10(d) show maps of the positions of spins ^{13}C relative to the NV centers of each of them, while the values of the components A_{xy} [Fig. 10(c)] and A_{zz} [Fig. 10(b)] are shown in color shades. Note that NV2 is located close to the magic-angle latitude with negligible A_{zz}, while the other three deviate significantly (note that values are presented on a logarithmic scale) from it.

Having in hand the results obtained for the ideal pair, we will briefly consider the problem associated with the presence of the $A_\parallel$ component, which arises due to the arbitrary arrangement in space of nuclear spins with respect to the electron spin.

As we discussed above, dephasing of nuclear spins is also subject to intrinsic dephasing with a ate Γ_{intr} and additional dephasing at a rate of Γ_{opt} caused by optical readout, which involves the longitudinal component $A_\parallel$ in the interaction. The total decay rate is then the sum of all contributions

$$\Gamma \approx \frac{\alpha^2}{4t_s} + \frac{1}{T_2^*} + \frac{A_\parallel^2 t_l^2}{2t_s} \approx \Gamma_\perp + \Gamma_2, \qquad (J1)$$

where $\Gamma_\perp$ is given by and Γ_2 is the decay rate determined by Γ_{intr} and Γ_{opt} and possibly by some additional perturbations. We estimate the values of Γ_2 for the ^{13}C-NV pairs by the following procedure.

Applying successive weak measurements of target spins with a preliminary polarization scheme [Fig. 7(a)] at different values of t_s for different pairs, we calculate the corresponding values of the total decay rate Γ. The values of the total decay rate as a function of t_s/α^2 are shown in Fig. 10(a), where the straight line with constant slope corresponds to the values of the back-action decay rate $\Gamma_\perp$. This line marks the
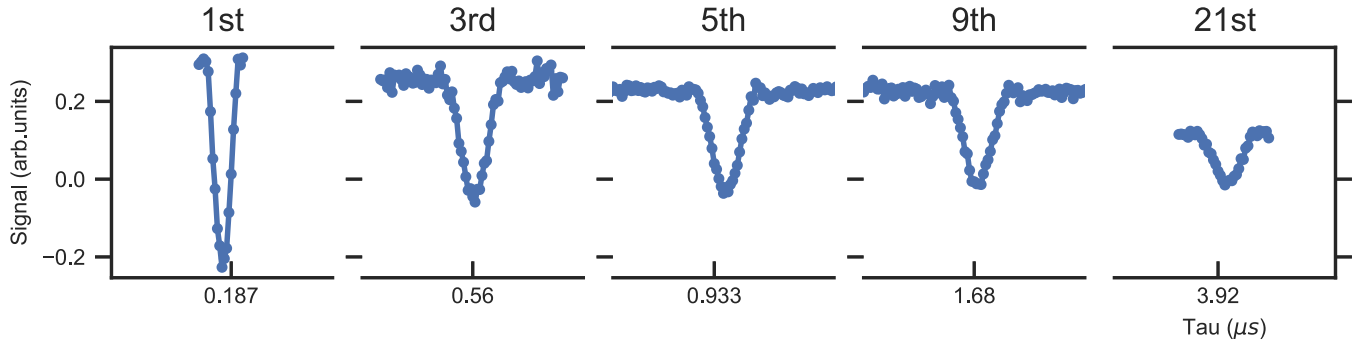
FIG. 15. High-order KDD-XY30 (totally $600\,\pi$ pulses) (maximum contrast) spectroscopy of the nuclear spin bath. No trace of A_{zz} coupling, though there is clear indication of negative contrast, caused by coherent interaction via the A_{zx} terms.

boundary of physically unreachable area (red) for quantum measurements. Note that the green dots corresponding to the NV2 pair almost exactly lie on this line, which in particular indicates that NV2 corresponds to the magic angle. From these data, with a reasonable assumption that the marks in the picture fluctuate around different constant values, we can estimate the approximate values of Γ_2 for different pairs of spins. In Fig. 10(b) the points marked with the symbols of the corresponding pairs are shown, the position of which is determined by the coordinates A_{zz} along the abscissa and the decay rate Γ_2 along the ordinate. The coordinates of the pair NV2 differ significantly from the coordinates of the other pairs, as a result of which the recorded processes differ sharply. This can be seen in Fig. 10, where, for comparison, the measurement results for pair NV11 and ideal pair NV2 are given. The noisy nature of the registered processes of all pairs except NV2 does not allow using them for a fine analysis of revealing purely quantum properties of the process. This fact, however, is not an obstacle to the use of the NV center in diamond in quantum sensor networks and distributed quantum computation.

APPENDIX K: EXPERIMENTAL SETUP AND DIAMOND SAMPLE

The experimental setup consists of a superconducting magnet (Scientific Magnetics) with a room temperature bore adjacent to a confocal microscope. The 12Gs AWG (Keysight M8190) p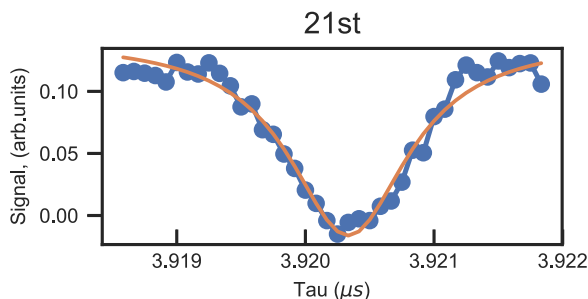rovides microwaves amplified with a traveling wave tube amplifier (Hughes 8010H) and radio frequencies amplified with an Amplifier Research 150A250 amplifier for control for the spin experiment. The optical readout is performed via a confocal microscope with 520 nm laser diode (Thorlabs) and APD (Perkin Elmer SPCM). The objective lens (NA = 1.35) is positioned via the 3D nonmagnetic piezo positioner (n-Point) (see Fig. 11). Photoluminescence is spatially filtered with a pinhole (50 um) and spectrally with a long-pass filter 650 nm (Semrock).

The $\langle 111 \rangle$-oriented diamond slice (2 mm × 2 mm × 88 μm) is obtained by laser cutting and polishing from a high crystalline quality, 99.995% ^{12}C-enriched, type IIa high-pressure and high-temperature (HPHT) crystal. In the original crystal, single NV centers were created by 2 MeV electron irradiation (1.3×10^{11} cm^{-2}) at room temperature and subsequent annealing (1000 °C for 2 h in vacuum). The sample is positioned on a coplanar waveguide to deliver the microwave and r.f. signal to the NV site (see Fig. 12). The B field is aligned with the NV orientation.

APPENDIX L: HYPERFINE FIELD CALIBRATION

To find a proper NV center for our experiment we examined around 20 NV centers and checked their nuclear spin environment. A set of calibration measurements for the NV center was used to calibrate the weakly coupled nuclear spin ^{13}C.

FIG. 16. Zoom into the 21st resonance of the KDD-XY30 sequence for the NV2. The resonance reveals no A_{zz} coupled nuclear spins and allows for determination of Larmor frequency with higher precision.
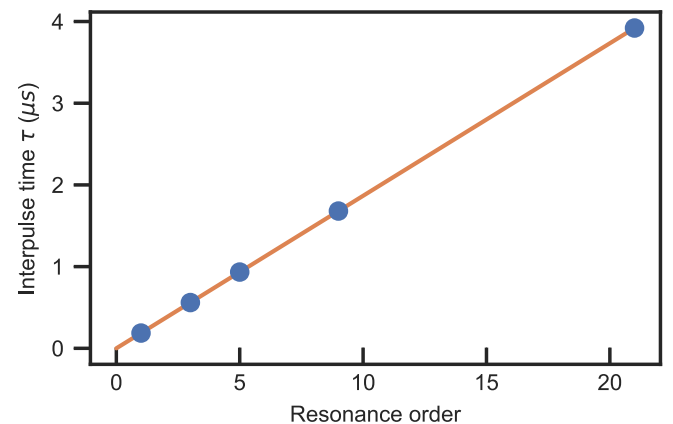

FIG. 17. DD resonance position in microseconds as a function of its order.
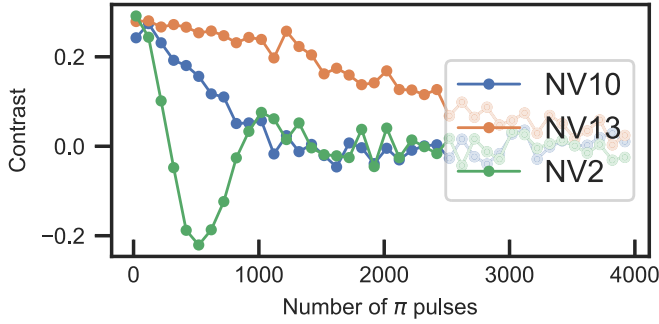
FIG. 18. Demonstration of coherent coupling in NV2. Dependence of the evolution on number of pulses in the KDD-N sequence shows the coherent oscillations for NV2, while for other NVs without a signal in the ENDOR sequence, the decay results in loss of coherence, meaning that the A_{zx} coupling is also weak.

1. ODMR

First, we examine the NV center ODMR spectrum and check that there is no strongly coupled ^{13}C spin by observing three peaks associated with the ^{14}N intrinsic nuclear spin (Fig. 13). This means that A_{zz} is below $1/(\pi T_\pi) \approx 30$ kHz, for $T_\pi = 8$ µs.

2. CSTE

Second, we examine the weakly coupled bath nuclei, using the ENDOR sequence [53] with total interrogation time $\tau = 100$ µs. In Fig. 14 we see that, e.g., for NV5 there is a moderately coupled nuclear spin with $A_{zz} = 10$ kHz coupling. For our experiments we search for NV centers, which do not have a detectable ENDOR signal for the ^{13}C nuclear spins, meaning that $A_{zz} \ll 10$ kHz, e.g., like for NV2 (Fig. 14, right panel).

3. KDD-N τ and N sweep

In addition to the absence of the ENDOR signal, we check the nuclear bath spectroscopy via high-order DD resonance [20]. By going to the highest possible resonance (in our case, 21st) with KDD-XY30 sequence, we determine no visible splitting of the ^{13}C bath peak (Figs. 15, 16). That means that the A_{zz} coupling is below 0.37 kHz. From the position of the peaks as a function of resonance number we determine the Larmor frequency with high precision (Fig. 17). Next, we check that the first peak has a coherent interaction by changing the number of pulses N in the KDD-N sequence and observe coherent oscillations for NV2 (Fig. 18).

We derive $\tau = 3.92033(2)$ µs from the best fit of the curve. From the fitting of Fig. 17, we got also the linear dependence of the resonance position as a function of its order: $a\,k + b$
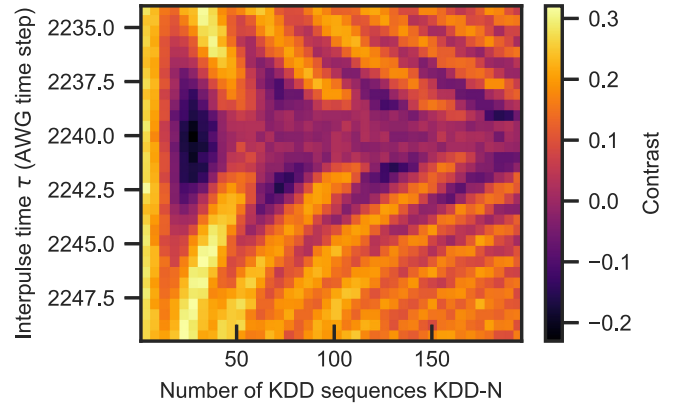

FIG. 19. 2D image of KDD numbers vs the interpulse time. The image shows a coherent evolution of the single weakly coupled nuclear spin. The resonance to the bath is also visible, resulting in dissipative dynamics.

with $a = 0.186682(1)$ and $b = 10^{-6}$. Having the value for the width of the 21st resonance we obtain an upper bound on the A_{zz} coupling as

$$\tau_k \approx \frac{(2k+1)\pi}{\omega_l + A_{zz}/2},$$

$$\delta\tau_k = \frac{(2k+1)2\pi}{2\omega_l + A_{zz}} - \frac{(2k+1)2\pi}{2\omega_l} \approx \tau_k \frac{A_{zz}}{\omega_l},$$

$$\frac{\delta\tau_k}{\tau_k} \approx \frac{A_{zz}}{\omega_l},$$

$$A_{zz} < \frac{\delta\tau_k}{\tau_k}\omega_l = 0.37(2\pi) \text{ kHz}. \tag{L1}$$

To further study the interaction with the bath, we obtain a 2D image of KDD-XY number and period of the interpulse sequence. The obtained figure resembles a 2D Rabi oscillations with detuning. It can be seen from Fig. 19 that during the DD, the NV is moderately coupled to a single nuclear spin via the A_{zx} interaction, which gives a coherent oscillation in a broad region of τ intervals, while the bath interaction results in coherence fast decay after the first full oscillation. As soon as the detuning of τ is larger than the average A_{zx} coupling to the bath, only coherent interaction is visible. The 2D data presented in Fig. 19 were fitted to extract the center of the fringes and the effective coupling to the nuclear spin. Results are presented in Table I.

4. Phase locking via τ sweep

To estimate the τ of the DD with higher precision we utilize a Hamiltonian interpolation technique [54]. Since the

TABLE I. Various method to estimate the hyperfine components of the single weakly coupled nuclear spin of NV2.

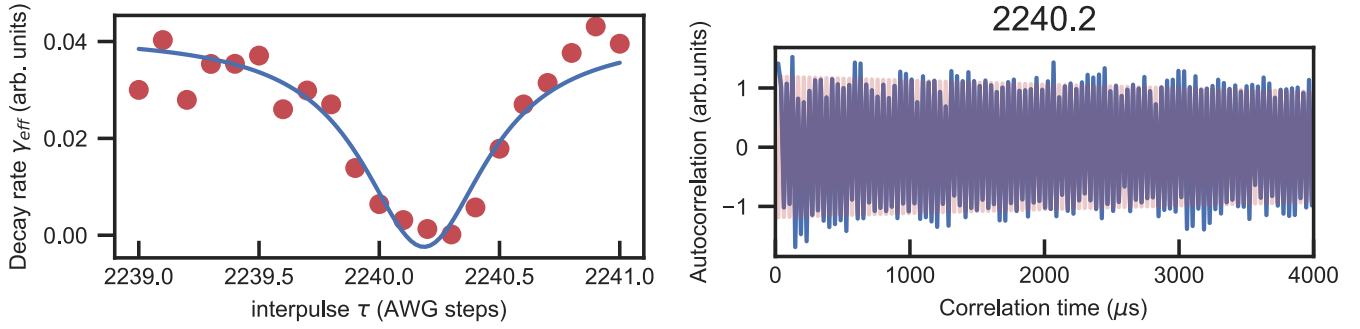|	CSTE (ENDOR)	First-order KDD-N Rabi (A_{zx}) Tau sweep 21st resonance (A_{zz})	Weak measurement decay	Phase locking in weak measurements	Correlation function fitting
A_{zx}, kHz	NA	9.4(2)	7.8(6)	7.9 (5)	9.5(7)
A_{zz}, kHz	$\ll 10$	<0.37	NA	NA	NA
τ, µs		0.186682(1)		0.18668(1)	

FIG. 20. Precise determination of resonant τ of the DD sequence. Left: dependence of the decay of the correlation function on the interpulse time τ. Right: the no-decay correlation function in the region of the phase-matching condition.

A_{zz} term is very subtle, its accurate identification requires a calibration to observe it via the sequential weak measurements and observe the decay of the correlation function, similar to [24]. At the resonance condition, a phase matching occurs, which results in reduction of the decay rate of the correlation function and a phase transition, a phase locking of the nuclear spin precession. We design a sequence, parametrized with τ, which, if τ is chosen correctly, is perfectly synchronized for phase matching. This results in a nuclear spin free precession angle between subsequent measurements equal to an odd number of π. Upon sweeping the τ of the DD we observe that

when the τ is resonant the correlation function is not decaying (see Fig. 20). The width of this resonance could be reduced with reducing the measurement strength. We find that $\tau = 2240.18(2)$ of AWG steps, or $\tau = 2240.18(2) \times 1/12 \, \text{ns} = 0.18668(1) \, \mu\text{s}$, which corresponds to the τ estimated from the slope as $\tau_{slope} = 0.186682(1) \, \mu\text{s}$ within the error bars.

5. Phase locking via t_f sweep

Alternatively, fixing the interpulse interval τ at resonance condition, and sweeping the free precession angle by precisely
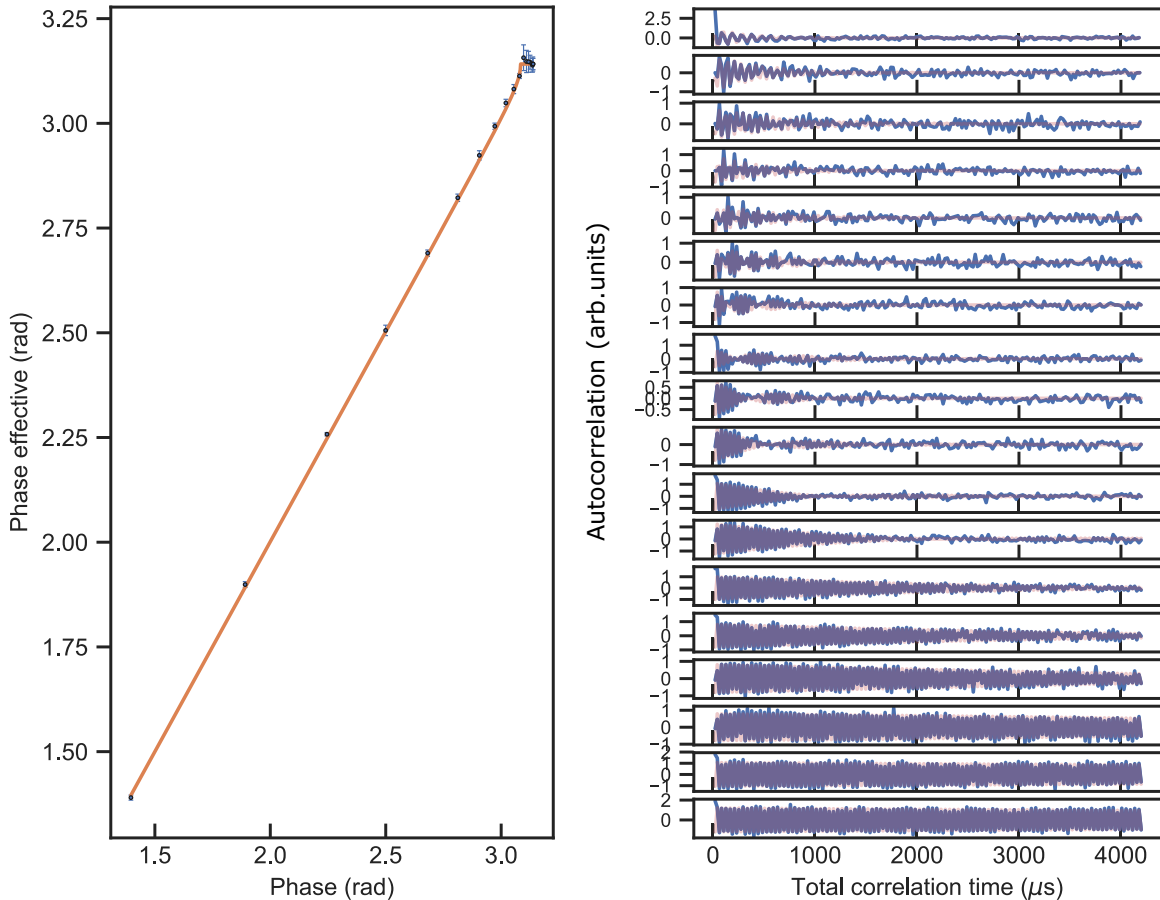

FIG. 21. Free precession angle sweeping, and phase-locking effect (left). The decay of the autocorrelation vanishes as the phase acquired by the target spin between successive measurements approaches π.
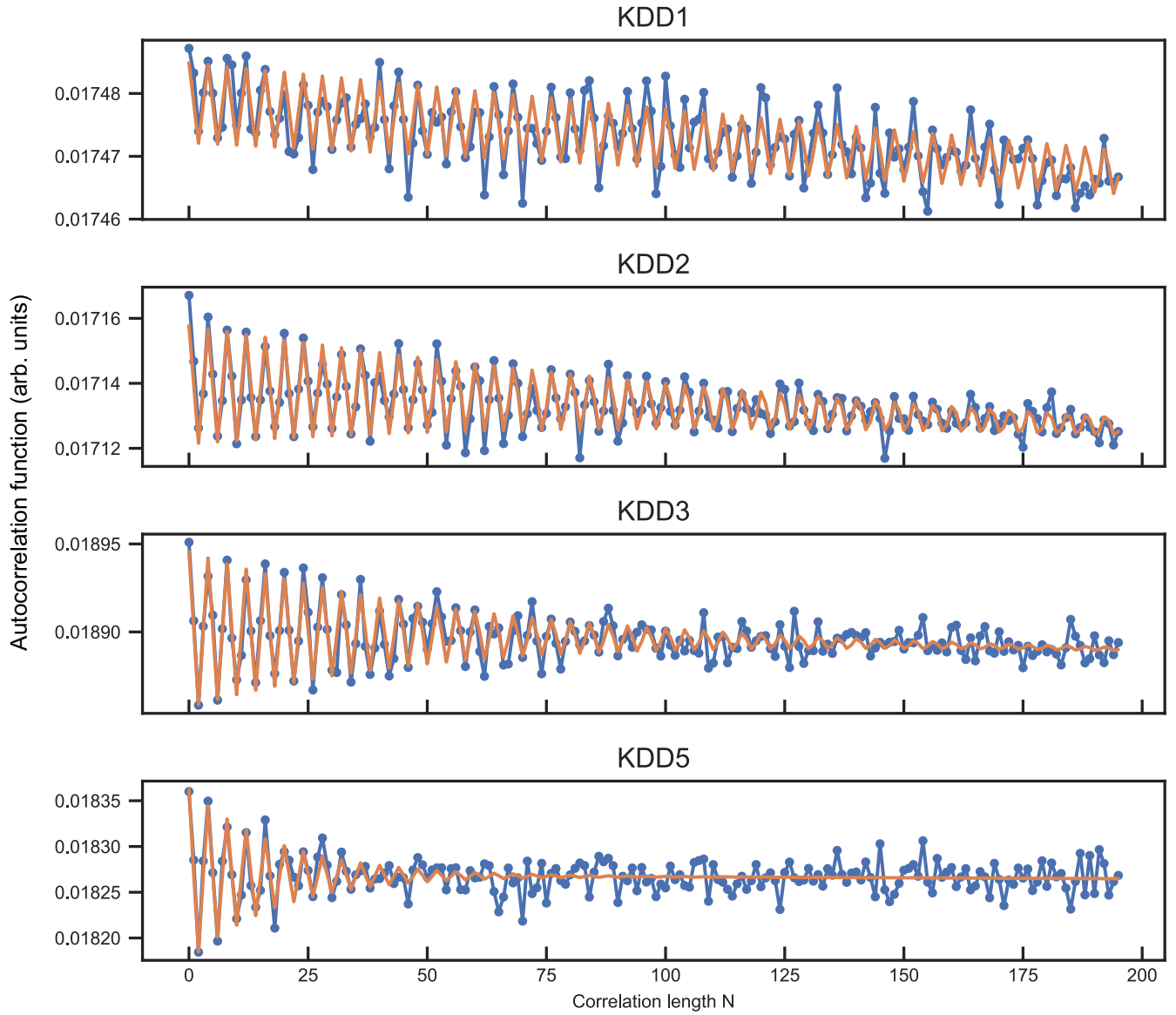
FIG. 22. Decay of the correlation function for KDD1, 2, 3, 5.

controlling the time interval added between the measurements, the phase-locking feature also allows us to make an estimate of the perpendicular component of the hyperfine term (see Fig. 21). As described in [24], the orange line was fitted with the curve which resulted in the value of A_{zx}. We provide the value and the error in Table I. For KDD-XY5:

$$\alpha = N_p A_{zx} \tau \pi = 0.14(1)\pi,$$
$$N_p = 100,$$
$$\tau = 2240.2/12 \text{ ns}. \quad \text{(L2)}$$

6. Measurement strength sweep

As shown in Fig. 22, we check the dependence of the decay of the correlation function on the measurement strength, i.e., the number of pulses. As a result, we fit the decay constant with $\alpha^2/4$ dependence, which gives us an approximate determination of the A_{zx} coupling (see Fig. 23).

APPENDIX M: PARAMETERS OF THE SEQUENCE

The sequence scheme timing (see Table II) is as follows:
(1) Repetitive readout (200 times)
   (a) Electron spin green laser readout time: 340 ns

TABLE II. Typical sequence scheme timing.

Repeated readout 200 times	Initial ^{14}N spin	Wait time	KDD	SWAP	Total time
CNOT for 1.07 µs + green laser for 300 ns + wait 0.5 µs ≈ 400 µs	≈151 µs	≈10 µs	≈35 µs	≈34 µs	≈630 µs

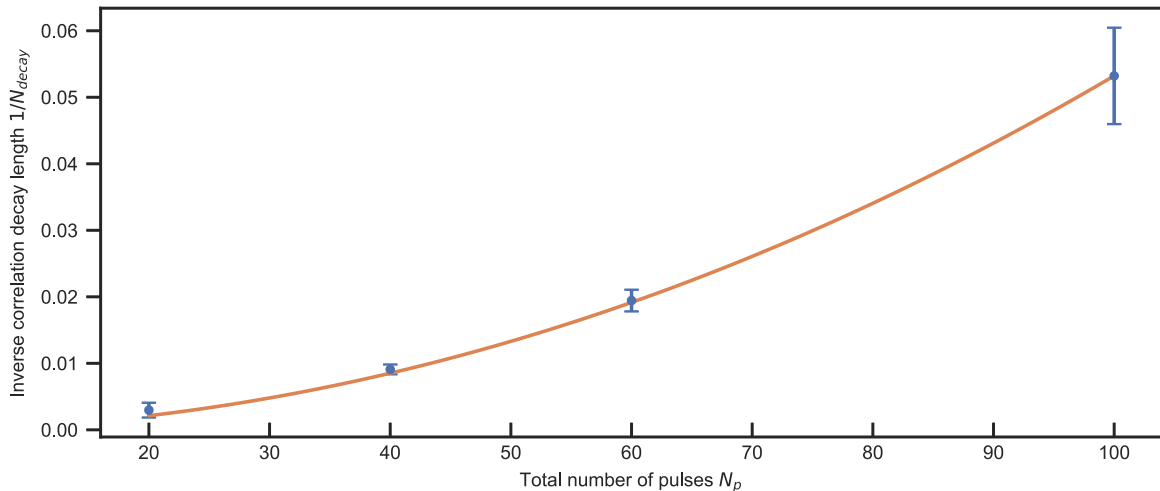FIG. 23. Decay of the correlation function as a function of the measurement strength.

(b) C_nROT_e to electron spin 1.07 μs
(2) ^{14}N polarization: 151 μs
   (a) C_nROT_e to electron spin 4 μs
   (b) C_eROT_n to nuclear spin 50 μs
   (c) Laser repolarization 300 ns
Repeat a, b, and c + 1μs wait time.

(3) 10 μs of waiting time
(4) KDD-XY5 is 35 μs
(5) C_eROT_n is 34 μs
The free precession time t_f is then estimated as the total time of the sequence, where CROT stands for controlled rotation.

[1] D. T. Smithey, M. Beck, M. G. Raymer, and A. Faridani, Measurement of the Wigner Distribution and the Density Matrix of a Light Mode using Optical Homodyne Tomography: Application to Squeezed States and the Vacuum, Phys. Rev. Lett. **70**, 1244 (1993).

[2] A. I. Lvovsky and M. G. Raymer, Continuous-variable optical quantum-state tomography, Rev. Mod. Phys. **81**, 299 (2009).

[3] A. Einstein, B. Podolsky, and N. Rosen, Can quantum-mechanical description of physical reality be considered complete? Phys. Rev. **47**, 777 (1935).

[4] W. Stulpe and P. Busch, The structure of classical extensions of quantum probability theory, J. Math. Phys. **49**, 032104 (2008).

[5] G. Birkhoff and J. von Neumann, The logic of quantum mechanics, Ann. Math. **37**, 823 (1936).

[6] M. Redei, *Quantum Logic in Algebraic Approach* (Kluwer, Dordrecht/Boston/London, 1998).

[7] A. M. Gleason, Projective topological spaces, Illinois J. Math. **12**, 482 (1958).

[8] L. G. Bunce and J .D. M. Wright, The Mackey-Gleason problem, Bull. Amer. Math. Soc. **26**, 288 (1992).

[9] E. P. Wigner, On hidden variables and quantum mechanical properties, Am. J. Phys. **38**, 1005 (1970).

[10] B. D'Espagnat, The quantum theory and reality, Sci. Am. **241**, 158 (1979).

[11] J. S. Bell, On the Einstein-Podolsky-Rosen paradox, Phys. Phys. Fiz. **1**, 195 (1964).

[12] J. S. Bell, On the problem of hidden variables in quantum mechanics, Rev. Mod. Phys. **38**, 447 (1966).

[13] D. Bohm, *Quantum Theory* (Prentice-Hall, Englewood Cliffs, NJ, 1951).

[14] A. J. Leggett and A. Garg, Quantum mechanics versus macroscopic realism: Is the flux there when nobody looks? Phys. Rev. Lett. **54**, 857 (1985); A. J. Leggett, Testing the limits of quantum mechanics: motivation, state of play, prospects, J. Phys.: Condens. Matter **14**, R415 (2002).

[15] K. Hess, H. De Raedt, and K. Michielsen, From Boole to Leggett-Garg: Epistemology of Bell-type inequalities, Adv. Math. Phys. **2016**, 4623040 (2016).

[16] I. Pitowsky, From George Boole to John Bell – The origins of Bell's inequality, *Bell's Theorem, Quantum Theory and Conceptions of the Universe*, edited by M. Kafatos, Fundamental Theories of Physics, Vol. 37 (Springer, Dordrecht, 1989), pp. 37–49.

[17] G. Boole died on December 8, 1864, exactly 100 years before Bell's article appeared.

[18] J. L. Doob, *Stochastic Processes* (Wiley, 1990).

[19] L. Robledo, H. Bernien, T. van der Sar, and R. Hanson, Spin dynamics in the optical cycle of single nitrogen-vacancy centres in diamond, New J. Phys. **13**, 025013 (2011).

[20] T. H. Taminiau, J. J. T. Wagenaar, T. van der Sar, F. Jelezko, V. V. Dobrovitski, and R. Hanson, Detection and Control of Individual Nuclear Spins Using a Weakly Coupled Electron Spin, Phys. Rev. Lett. **109**, 137602 (2012)

[21] M. Doherty *et al.*, The nitrogen-vacancy colour centre in diamond, Phys. Rep. **528**, 1 (2013).

[22] P. Neumann, J. Beck, M. Steiner, F. Rempp, H. Fedder, P. R. Hemmer, J. Wrachtrup, and F. Jelezko, Single-shot readout of a single nuclear spin, Science **329**, 542 (2010).

[23] N. Imoto, H. A. Haus, and Y. Yamamoto, Quantum nondemolition measurement of the photon number via the optical Kerr effect, Phys. Rev. A **32**, 2287 (1985).

[24] M. Pfender, P. Wang, H. Sumiya, S. Onoda, W. Yang, D. B. R. Dasari, P. Neumann, X. Y. Pan, J. Isoya, R. B. Liu, and J. Wrachtrup, High-resolution spectroscopy of single nuclear

spins via sequential weak measurements, Nat. Commun. **10**, 594 (2019).

[25] K. S. Cujia, J. M. Boss, K. Herb, J. Zopes, and C. L. Degen, Tracking the precession of single nuclear spins by weak measurements, Nature (London) **571**, 230 (2019).

[26] C. Emary, N. Lambert, and F. Nori, Leggett-Garg inequalities, Rep. Prog. Phys. **77**, 016001 (2014).

[27] A. Palacios-Laloy, F. Mallet, F. Nguyen, P. Bertet, D. Vion, D. Esteve, and A. N. Korotkov, Experimental violation of a Bell's inequality in time with weak measurement, Nat. Phys. **6**, 442 (2010).

[28] G. Waldherr, P. Neumann, S. F. Huelga, F. Jelezko, and J. Wrachtrup, Violation of a Temporal Bell Inequality for Single Spins in a Diamond Defect Center, Phys. Rev. Lett. **107**, 090401 (2011) ; Publishers Note: Violation of a Temporal Bell Inequality for Single Spins in a Diamond Defect Center [Phys. Rev. Lett. 107, 090401 (2011)], **107**, 129901(E) (2011).

[29] W.-L. Ma and R.-B. Liu, Angstrom-Resolution Magnetic Resonance Imaging of Single Molecules via Wave-Function Fingerprints of Nuclear Spins, Phys. Rev. Appl. **6**, 024019 (2016).

[30] J. Boss, K. Chang, J. Armijo, K. Cujia, T. Rosskopf, J. R. Maze, and C. L. Degen, One- and Two-Dimensional Nuclear Magnetic Resonance Spectroscopy with a Diamond Quantum Sensor, Phys. Rev. Lett. **116**, 197601 (2016).

[31] J. Grabowski *et al.*, Geometry of quantum systems: Density states and entanglement, J. Phys. A: Math. Gen. **38**, 10217 (2005).

[32] N. Gisin, Bell's inequality holds for all non-product states, Phys. Lett. A **154**, 201 (1991).

[33] M. Horodecki, P. Horodecki, and R. Horodecki, Mixed-State Entanglement and Distillation: Is there a "Bound" Entanglement in Nature? Phys. Rev. Lett. **80**, 5239 (1998).

[34] R. F. Werner and M. M. Wolf, Bell inequalities and entanglement, Quantum Inf. Comput. **1**, 1 (2001).

[35] M. Kus and K. Zyczkowski, Geometry of entangled states, Phys. Rev. A **63**, 032307 (2001).

[36] E. B. Davis, *Quantum Theory of Open Systems* (Academic Press, 1976).

[37] K. Kraus, States, *Effects and Operations: Fundamental Notions of Quantum Theory* (Springer-Verlag, 1983).

[38] A. S. Holevo, *Statistical Structure of Quantum Theory* (Springer-Verlag, 2001).

[39] T. H. Taminiau, J. Cramer, T. van der Sar, V. V. Dobrovitski, and R. Hanson, Universal control and error correction in multi-qubit spin registers in diamond, Nat. Nanotechnol. **9**, 171 (2014).

[40] J. R. Klauder and E. C. G. Sudarshan, *Fundamentals of Quantum Optics* (W.A. Benjamin, New York, 1968).

[41] J. Gambetta *et al.*, Quantum trajectory approach to circuit QED: Quantum jumps and the Zeno effect, Phys. Rev. A **77**, 012112 (2008).

[42] G. Lindblat, On the generators of quantum dynamical senigroups, Commun. Math. Phys. **48**, 119 (1976).

[43] V. Gorini, A. Kossakowski, and E. C. G. Sudarshan, Completely positive dynamical semigroups of *N*-level systems, J. Math. Phys. **17**, 821 (1976).

[44] E. B. Davies, Markovian master equations, Commun. Math. Phys. **39**, 91 (1974).

[45] M. Steiner, P. Neumann, J. Beck, F. Jelezko, and J. Wrachtrup, Universal enhancement of the optical readout fidelity of single electron spins at nitrogen-vacancy centers in diamond, Phys. Rev. B **81**, 035205 (2010).

[46] A. Gupta, L. Hacquebard, and L. Childress, Efficient signal processing for time-resolved fluorescence detection of nitrogen-vacancy spins in diamond, J. Opt. Soc. Am. B **33**, B28 (2016).

[47] H. J. Groenewold, On the principles of elementary quantum mechanics, Physica **12**, 405 (1946).

[48] M. L. Goldman, A. Sipahigil, M. W. Doherty, N. Y. Yao, S. D. Bennett, M. Markham, D. J. Twitchen, N. B. Manson, A. Kubanek, and M. D. Lukin, Phonon-Induced Population Dynamics and Intersystem Crossing in Nitrogen-Vacancy Centers, Phys. Rev. Lett. **114**, 145502 (2015).

[49] S. Adhikari, Constructing a ball of separable and absolutely separable states for quantum system, Eur. Phys. J. D **75**, 92 (2021).

[50] S. Kullback and R. A. Leibler, On information and sufficiency, Ann. Math. Stat. **22**, 79 (1951).

[51] I. Schwartz, J. Scheuer, B. Tratzmiller, S. Müller, Q. Chen, I. Dhand, Z. Y. Wang, C. Müller, B. Naydenov, F. Jelezko, and M. B. Plenio, Robust optical polarization of nuclear spin baths using Hamiltonian engineering of nitrogen-vacancy center quantum dynamics, Sci. Adv. **4**, eaat8978 (2018).

[52] See Supplemental Material at http://link.aps.org/supplemental/10.1103/PhysRevA.107.042212 for data analysis code.

[53] S. Zaiser, T. Rendler, I. Jakobi, T. Wolf, S. Y. Lee, S. Wagner, and P. Neumann, Enhancing quantum sensing sensitivity and spectral resolution by a quantum memory, Nat. Commun. **7**, 12279 (2016).

[54] A. Ajoy, Y. X. Liu, K. Saha, L. Marseglia, J. C. Jaskula, U. Bissbort, and P. Cappellaro, Quantum interpolation for high-resolution sensing, Proc. Natl. Acad. Sci. USA **114**, 2149 (2017).